frontiers | Frontiers in Chemistry

TYPE Review
PUBLISHED 08 August 2022
DOI 10.3389/fchem.2022.959422

OPEN ACCESS

EDITED BY
Shanhui Zhu,
Institute of Coal Chemistry (CAS), China

REVIEWED BY
Maria A. Goula,
University of Western Macedonia, Greece
Miriam Navlani-García,
University of Alicante, Spain

*CORRESPONDENCE
Yulian He,
yulian.he@sjtu.edu.cn

†These authors share first authorship

SPECIALTY SECTION
This article was submitted to Catalytic Reactions and Chemistry, a section of the journal Frontiers in Chemistry

RECEIVED 01 June 2022
ACCEPTED 28 June 2022
PUBLISHED 08 August 2022

CITATION
Gao Y, Jiang M, Yang L, Li Z, Tian F-X and He Y (2022), Recent progress of catalytic methane combustion over transition metal oxide catalysts.
Front. Chem. 10:959422.
doi: 10.3389/fchem.2022.959422

Recent progress of catalytic methane combustion over transition metal oxide catalysts

Yuan Gao[1†], Mingxin Jiang[1†], Liuqingqing Yang[1], Zhuo Li[1], Fei-Xiang Tian[2] and Yulian He[1,3*]

[1]UM-SJTU Joint Institute, Shanghai Jiaotong University, Shanghai, China, [2]State Key Laboratory of Chemical Engineering, East China University of Science and Technology, Shanghai, China, [3]Department of Chemical Engineering, Shanghai Jiao Tong University, Shanghai, China

Methane (CH_4) is one of the cleanest fossil fuel resources and is playing an increasingly indispensable role in our way to carbon neutrality, by providing less carbon-intensive heat and electricity worldwide. On the other hand, the atmospheric concentration of CH_4 has raced past 1,900 ppb in 2021, almost triple its pre-industrial levels. As a greenhouse gas at least 86 times as potent as carbon dioxide (CO_2) over 20 years, CH_4 is becoming a major threat to the global goal of deviating Earth temperature from the +2°C scenario. Consequently, all CH_4-powered facilities must be strictly coupled with remediation plans for unburned CH_4 in the exhaust to avoid further exacerbating the environmental stress, among which catalytic CH_4 combustion (CMC) is one of the most effective strategies to solve this issue. Most current CMC catalysts are noble-metal-based owing to their outstanding C−H bond activation capability, while their high cost and poor thermal stability have driven the search for alternative options, among which transition metal oxide (TMO) catalysts have attracted extensive attention due to their Earth abundance, high thermal stability, variable oxidation states, rich acidic and basic sites, etc. To date, many TMO catalysts have shown comparable catalytic performance with that of noble metals, while their fundamental reaction mechanisms are explored to a much less extent and remain to be controversial, which hinders the further optimization of the TMO catalytic systems. Therefore, in this review, we provide a systematic compilation of the recent research advances in TMO-based CMC reactions, together with their detailed reaction mechanisms. We start with introducing the scientific fundamentals of the CMC reaction itself as well as the unique and desirable features of TMOs applied in CMC, followed by a detailed introduction of four different kinetic reaction models proposed for the reactions. Next, we categorize the TMOs of interests into single and hybrid systems, summarizing their specific morphology characterization, catalytic performance, kinetic properties, with special emphasis on the reaction mechanisms and interfacial properties. Finally, we conclude the review with a summary and outlook on the TMOs for practical CMC applications. In addition, we also further prospect the enormous potentials of TMOs in producing value-added chemicals beyond combustion, such as direct partial oxidation to methanol.

KEYWORDS

methane, catalytic combustion, heterogeneous catalysis, transition metal oxide, reaction mechanism

1 Introduction

CH_4 is the cleanest fossil fuel with the highest energy content (50–55 MJ/kg) among all sources. It emits 50–60% less CO_2, ~ 80% less nitrogen oxides (NO_x), and almost negligible amount of toxic air pollutants including SO_x, Hg, and PM 2.5 compared to that of coals (He L. et al., 2020; Zhang et al., 2021). Today, it has been well recognized that CH_4 will play an indispensable role in the paradigm shift to a more sustainable planet. However, as the main component of natural gas, CH_4 is the second-largest greenhouse gas after CO_2 with a global warming potential almost 86 times that of CO_2 over 20 years (He Y. L. et al., 2020).

Since the beginning of the industrial revolution, CH_4 emissions have raced past 1,900 ppb in 2021, almost triple its pre-industrial levels, and contributed about 20% to the global greenhouse effect so far (Pratt and Tate, 2018; Palella et al., 2021). Specifically in China, circumstances like the incomplete combustion of fossil fuels, natural gas extraction, animal enteric fermentation, crop cultivation, agricultural residue incineration, and solid waste landfills, etc., have resulted in an annual atmospheric CH_4 emission taking up about 60% of the total non-CO_2 greenhouse gas emissions (Teng et al., 2019; Gong and Zeng, 2021). In this sense, the environmental benefits of CH_4 resource itself will be largely balanced by the unburned emission, if no strict remediation plan in the exhaust stream is considered.

Catalytic combustion is one of the most effective means for CH_4 utilization for both clean power generation and emission control (Setiawan et al., 2015; Seeburg et al., 2018). Compared to the traditional flame combustion, where high operational cost and toxic substances such as carbon monoxide (CO) and NO_x caused by the high combustion temperatures (>1,400°C) are almost inevitable (Stoian et al., 2021), flameless combustion of CH_4 under the aid of a solid catalyst allows for not only a much lower operation temperature and much reduced NO_x emission but also a wider range of air-to-fuel ratio with a more stable and efficient combustion process outside the combustion limits (He L. et al., 2020).

At the heart of the CMC reaction lies the development of combustion catalysts, of which the catalytic performance and the cost should be properly balanced for practical implementations. To date, the most extensively explored CMC catalysts are precious metals like palladium, platinum, and rhodium, as is the case in the three-way catalytic converter for emission control in automobiles (Choya et al., 2021).

Noble metal catalysts are typically good at activating the C–H and O–O bonds to form free radicals and triggering the chain reactions, thus driving CMC to a low-temperature regime, while their high cost has never stopped the community searches for promising alternatives of cheaper price (Liu et al., 2015). Over the past decades, TMOs have received tremendous attention as one of the most promising candidates for catalyzing CMC owing to their great Earth abundance, low toxicity, and many outstanding physiochemical properties. Comparable, if not superior, performance to noble-metal-based systems has been reached in some cases such as Fe_2O_3, Co_3O_4, etc., (Li J. A. et al., 2019; He Y. L. et al., 2020; Zheng Y. F. et al., 2020; Yang et al., 2022), while with that being said, their practical uses are still limited by the low-temperature activity, resistivity against water, and sulfur tolerance in the combustion environment. Further improvement of the catalytic performance of TMO catalysts would require a well understanding of the active site structures and the corresponding reaction mechanisms, which unfortunately still remain largely controversial at the current stage, primarily due to 1) the high structural complexity of oxides themselves, involving a variety of surface acidic and basic sites; 2) the competitions between lattice oxygen and the molecular oxygen as the oxidizing sources; 3) oxygen exchange behaviors at the solid–gas interface; and 4) various adsorbed oxygen species (Toscani et al., 2019).

This review presents a systematic compilation of TMO-catalyzed CMC with special focus on the reaction mechanisms. We start with a brief introduction of the scientific fundamentals of the CMC reaction. Then, we move on to discuss the unique and desirable features of TMOs for the CMC reaction and different CH_4 activation pathways, followed by a detailed introduction of four different kinetic reaction models. Next, we categorize the TMOs of interests into single and mixed systems, summarizing their specific morphology characterization, catalytic performance, kinetic properties, with special emphasis on the reaction mechanisms and interfacial properties. Finally, we conclude the review with a summary and outlook on the TMOs for practical CMC applications. Last but not least, we also further prospect the enormous potentials of TMOs beyond CMC, such as partial oxidation to value-added chemicals.

2 Reaction fundamentals

2.1 Catalytic CH_4 combustion reaction

CH_4 is an extremely stable and highly symmetrical tetrahedral structure formed by four identical C–H bonds. In CH_4, the sp^3-hybridized carbon atom locates in the center of the regular tetrahedron, and four hydrogen atoms are distributed on the respective four vertices. CH_4 possesses a high ionization potential (12.5 eV), a low electron affinity (4.4 eV), and a high C–H bond energy (434 kJ/mol), rendering both the nucleophilic and electrophilic attacks on CH_4 extremely challenging under

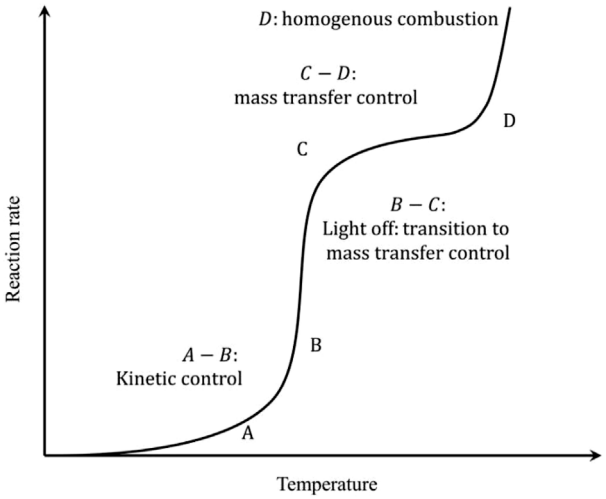

FIGURE 1
The reaction rate of CMC as a function of temperature. Reprinted with permission from He L. et al. (2020). Copyright (2020) Elsevier.

mild conditions (Vickers et al., 2015). The complete oxidation of CH_4 proceeds through the following reaction (1):

$$CH_4 + 2O_2 = CO_2 + 2H_2O\ \Delta H_{(298K)} = -803\ kJ/mol \quad (1)$$

As the combustion reaction is highly exothermic, side reactions such as CH_4–CO_2 reforming (Eq. 2), CH_4-steam reforming (Eq. 3), reverse water gas shift reaction (Eq. 4), partial oxidation (Eq. 5), and water gas shift reaction (Eq. 6) are almost inevitable at high temperature, as shown in the following reactions (Horn and Schlögl, 2014):

$$CH_4 + CO_2 = 2CO + 2H_2\ \Delta H_{(298K)} = 247\ kJ/mol \quad (2)$$

$$CH_4 + H_2O = 3H_2 + CO\ \Delta H_{(298K)} = 205.7\ kJ/mol \quad (3)$$

$$CO_2 + H_2 = CO + H_2O\ \Delta H_{(298K)} = 41.1\ kJ/mol \quad (4)$$

$$CH_4 + 1/2O_2 = CO + 2H_2\ \Delta H_{(298K)} = -36\ kJ/mol \quad (5)$$

$$CO + H_2O = H_2 + CO_2\ \Delta H_{(298K)} = -41.9\ kJ/mol \quad (6)$$

In the 1970s, Pfefferle *et al.* proposed the process of "heterogeneous catalytic combustion" (Pfefferle and Pfefferle, 1987), where a solid catalyst can be used to combust CH_4 in a flameless manner at a much lower reaction temperature (<500°C). Compared with traditional homogeneous flame combustion, the catalytic process owns advantages such as low light-off temperatures, reduced pollutant emission, wide operation ranges, and lower reactor requirement.

The CMC involves heterogeneous reactions, where complex processes such as mass transfer and heat transfer occur between the catalyst surface and the gas phase. Figure 1 shows the schematic relation between the reaction rate and temperature of CMC (He L. et al., 2020).

First part of the curve (A–B) is the kinetic-control zone, in which the reaction rate increases slowly with reaction temperature. At low temperatures, the reaction is limited by the intrinsic kinetics such as the dissociation rate of reactants over the catalytic surfaces. The second part of the curve (B–C) is known as the light-off regime where the reaction rate increases almost exponentially with the increase of the temperature. This is due to the drastic increase of the intrinsic reaction kinetics so that the overall reaction rates gradually transition to be controlled by the mass transfer rates. Upon further increase of the temperature (C–D), the mass transfer finally becomes the rate-limiting step, and there appears the rate plateau. The final part of the curve (D) falls under the regime of homogeneous combustion, where high temperature triggers the free radical formation and the chain reaction directly in the gas phase. The latter two high-temperature regimes impose strict requirements on the reactor design to maintain the catalyst structural stability as well as the sufficient mass and heat transfer rates. A more desirable operation window should fall nearby the light-off regime for milder reaction temperatures and sufficiently high reaction rates.

In CMC, other substances like water and sulfur are easy to get adsorbed onto catalyst surfaces under actual operation conditions; thus, the desirable catalysts for CMC should also possess a good anti-water and anti-sulfur poisoning ability beyond high low-temperature activity and thermal stability. In addition, the economic aspects should also be taken into considerations when it comes to large-scale applications.

2.2 Transition metal oxides

TMOs are one of the most important classes of solid catalysts that have been extensively used in a variety of important industrial processes, such as the water gas shift reaction, CO oxidation, methanol synthesis, etc., owing to their excellent thermal stability, variable valence states, and Earth abundance (Tepamatr et al., 2016; Arena et al., 2017; Huang et al., 2021). In water-containing feed, the surface of TMOs undergo acid–base reaction to form surface hydroxyl groups, which react with other reactants *via* proton or electron transfer (Yang et al., 2022). Transition metal elements could easily alternate between the low oxidation state and the high oxidation state, thus allowing for a facile release and restoration of the lattice oxygen *via* a redox cycle (Chen et al., 2015). Such redox and acid–base properties have rendered TMOs to be one of the most promising candidates for CMC reactions.

TMOs like Co_3O_4, Fe_2O_3, MnO_2, etc., have shown catalytic activities comparable to that of noble metal-based systems in CMC (Pu et al., 2017; He Y. L. et al., 2020; Yang et al., 2021), while the performance can be largely affected by preparation method, carrier, doping, and experimental conditions (such as the presence of water vapor and sulfur). The most common preparation methods of TMOs include thermal decomposition,

precipitation, combustion synthesis, hydrothermal method, dipping, and sol–gel method (Tang et al., 2008). The different preparation methods can lead to diverse structural properties such as particle size, dispersion, surface area, morphology, crystal plane, metal valence states, defects, and reactive oxygen species. Such variances in the TMO crystal structures may result in drastic differences in the expression of catalytic activity, as was found in Co_3O_4, Fe_2O_3, IrO_2, etc., where only certain crystal facets are reactive for CMC reactions (Liang et al., 2017; He L. et al., 2020).

The main exposed crystal planes of TMOs with different morphologies have a significant effect on the catalytic activity of CMC. For example, the (111) and (112) crystal planes of Co_3O_4 and the (110) crystal planes of Fe_2O_3 are considered to be the best catalytic activity for CMC (Hu et al., 2008; He L. et al., 2020). In addition, the structure dimensionality also induces different catalytic properties due to quantum confinement and geometric effect, as was seen in Co_3O_4 where the 2D nanosheets and 3D nanoflowers possess drastically different catalytic performances (Jia Y. C. et al., 2016).

TMO-based catalysts are generally supported in CMC for improved particle dispersion, increased specific surface area, and enhanced catalytic performance. Both inactive and active supports are used to disperse TMOs in CMC. For example, Al_2O_3, as an inactive support, is an acidic oxide capable of adsorbing CH_4 through acid–base pairing (Wang and Lin, 2004; Choya et al., 2018a). Active supports, such as CeO_2, can directly participate in the CMC reaction through its excellent oxygen storage capacity (Pecchi et al., 2005; Li Y. X. et al., 2009).

Doping TMOs with an impurity element is also an effective strategy to improve their catalytic performance in CMC by inducing a great deal of lattice defects, acidic and basic sites, oxygen vacancies, synergistic effect, etc., (Li J. H. et al., 2009). The increased amount of oxygen vacancies can not only improve the mobility of bulk oxygen in the lattice but also creates additional adsorption sites to promote the molecular adsorption from the gas phase, reducing the activation barrier (Wang H. W. et al., 2019). The dopants in TMOs include metal and non-metal elements. Elements like Ca and Mg are often used as promoters, while Ce and Mn are doped to obtain oxygen vacancies (Pecchi et al., 2011; Chen Y. L. et al., 2021). N is a commonly used dopant in non-metal doping, which can create more lattice distortions and further increase active oxygen species (Buchneva et al., 2012; Li et al., 2018).

One of the most serious issues for TMO catalysts in CMC is their resistance to water poisoning. Most polar facets of TMOs are prone to dissociatively adsorb moisture through an acid–base reaction and form rich surface hydroxyl groups, while this process is highly reversible and self-dehydration can occur at elevated temperatures (He Y. L. et al., 2020). Water vapor on the surface of TMOs reacts with chemisorbed oxygen, which hinder the delivery of reactive oxygen species to active sites. Moreover, the formation of hydroxyl groups hinders the desorption of H_2O and CO_2 from the surface of TMOs (He L. et al., 2020). Water vapor poisoning is generally reversible owing to the competitive adsorption of water molecules with reactants. Some TMOs possess inherent water tolerant stability, such as NiO, owing to the modification of water for NiO. Tuning the structure and surface topography of the TMO catalysts is effective in obtaining resistance to water vapor (Liu et al., 2017; Xu et al., 2017). Hydrophobic modification of TMOs or their supports may also be an effective means to improve the water resistance and catalytic activity of catalysts (Kuo et al., 2014).

Sulfur poisoning is another serious issue for TMO catalysts in CMC. Natural gas contains a substantial amount of sulfur element, which can be oxidized into sulfur dioxide (SO_2) and get adsorbed onto the catalyst surface of the catalyst; subsequent oxidation to sulfate could also occur and thus cause serious sulfur poisoning. Some TMOs, such as Cr_2O_3, inherently have excellent sulfur resistance due to its low affinity to acid gases (Ordóñez et al., 2008). Sacrificial component such as Mn-based oxide can be used to guarantee the sulfur resistance of the CMC catalyst (Zhong et al., 2019). Similarly, supports such as Al_2O_3 can react with SO_2 to form sulfates, which protects active sites. But it is unfavorable for the recovery of TMO catalysts. In fuel-rich conditions, an elevated temperature (>500°C) is an effective means of recovery for sulfur-poisoned TMO catalysts (Gremminger et al., 2017).

In addition, carbon deposition can also cause serious catalyst deactivation in CMC, as commonly seen in carbonaceous reactions. Note that the effect can be remediated through carefully controlled reaction conditions, such as adjusting the air-to-fuel ratio, the space velocity, and the reaction temperature. In lean combustion scenario where the oxygen content is in excessive amount, the CH_n species formed from CH_4 dissociation can be rapidly oxidized by dioxygen to form CO_2, thus avoiding coke formation. While if a rich fuel mixture is used, the insufficient oxygen content can result in the formation of coke-like carbon (Tao et al., 2015). Under the circumstance of oxygen source coming from lattice oxygen rather than the molecular oxygen in the gas phase, the CH_4 to TMO catalyst feed ratio should be instead taken in consideration correspondingly. When the lattice oxygen in the TMO catalysts is insufficient to react with CH_4, CH_4 will decompose and then form carbon deposition (Wu and Ku, 2018). Another factor that can induce the catalyst deactivation is the space velocity, a small space velocity of the feed can lead to serious carbon deposition due to the long residence time between CH_n species and the catalysts (He Y. L. et al., 2020). Furthermore, carbon deposition may also result from the decomposition of CH_4 at high temperatures. Promoting coke oxidation can prolong the lifetime of TMO catalysts. TMOs with high

oxygen storage capacity such as CeO_2 can remove coke deposition through the release of lattice oxygen (Wang Y. N. et al., 2022). Therefore, sufficient oxygen content, reasonably short residence time, and low reaction temperature are necessary to reduce carbon deposition in CMC. For TMOs, in particular, a high oxygen storage capacity will be helpful to prevent coke formation.

2.3 Reaction mechanisms

The reaction mechanisms proposed for CMC over many TMOs remain to be controversial, primarily due to the high structural complexity, different oxygen sources, oxygen-exchange behaviors, etc. Such knowledge gaps hinder us from understanding the precise active site structures and the reaction pathways from a molecular level and consequently the optimization of TMO catalysts for CMC. To this end, the existing mechanistic studies of CMC over TMOs are summarized in this section.

2.3.1 C–H and O–O activation

Dissociation of the first C–H bond is the most critical step of CH_4 activation and the following CMC reactions (Feyel et al., 2006). Fu *et al.* studied different C–H activation mechanisms over various TMOs using cluster model calculations. It was found that H abstraction is the primary working mechanism for the activation of CH_4 on most TMOs such as Cr_3O_9 and Mo_3O_9, following the hydrogen atom transfer (HAT) route. H abstraction is a single-electron transfer process forming free radicals *via* the homolytic cleavage of the C–H bond, in which the H atom attacks the terminal oxygen atom from both *trans* and *cis* directions. In terms of activation energy, the H abstraction process in *trans* on the terminal oxygen is more favorable than that from the *cis* directions (Fu et al., 2006). Li *et al.* believed that there is also a proton-coupled electron transfer (PCET) process for the activation of C–H bonds on TMOs, that is, transition metal oxide ions and O^{2-} as a Lewis acid–base pair are served as catalytic active sites. In the process, a proton is abstracted from CH_4 by the Lewis basic O^{2-}, while the methyl anion is transferred to the Lewis-acidic metal center (Li et al., 2016). Thus, the activation of CH_4 on TMOs is usually closely related to the acidity and alkalinity of the surface.

In addition to CH_4 activation, the molecular oxygen also plays a significant role in governing the catalytic performance in CMC. The composition and concentration of reactive oxygen species significantly affect the CMC reaction over TMOs. In CMC, there are primarily two types of oxygen species involved in the TMOs, including surface-adsorbed oxygen and lattice oxygen. According to Eq. 7, the dissociative adsorption of molecular oxygen will result in the formation of a series of different adsorbed oxygen species with electrophilic characters, in the sequence of superoxide O_2^-, peroxide O_2^{2-}, and charged atomic species O^-. The reaction ultimately leads to the incorporation of nucleophilic O^{2-} into the lattice to form lattice oxygen (Wang Y. Q. et al., 2022). It is precisely because of the different activation forms of C–H bonds and oxygen molecules that the mechanism of CMC is such diverse

$$O_2(g) \overset{*}{\leftrightarrows} O_2(s) \overset{e^-}{\leftrightarrows} O_2^-(s) \overset{e^-}{\leftrightarrows} O_2^{2-}(s) \overset{*}{\leftrightarrows} 2O_2^-(s) \overset{2e^-}{\leftrightarrows} + 2V_0 2O^{2-} \quad (1)$$

$*$ – a free adsorption site;
g – gas surface; l – lattice

(7)

2.3.2 Kinetic models

The various forms of C–H and O–O activation mechanisms undoubtedly result in a complex reaction network for TMO-catalyzed CMC systems. According to the participation forms of different oxygen species, the proposed reaction mechanisms of the CMC currently include the following four mechanisms (Figure 2). Langmuir–Hinshelwood (L–H) mechanism and the Eley–Rideal (E–R) mechanism are dominated by surface-adsorbed oxygen, while the Mars van Krevelen (MvK) mechanism is dominated by lattice oxygen, and the two-term (T-T) mechanism is cooperatively controlled by the L–H mechanism and the MvK mechanism. The rate equations consistent with these mechanisms are as follows:

$$r_{LH} = k_C \frac{K_C P_C \cdot K_O P_O}{(1 + K_C P_C)(1 + K_O P_O)} \quad (8)$$

$$r_{ER} = k_O \frac{K_O P_O \cdot P_C}{(1 + K_O P_O)} \quad (9)$$

$$r_{MvK} = \frac{k_C P_C \cdot k_O P_O}{v k_C P_C + k_O P_O} \quad (10)$$

L–H mechanism. It is believed that the adsorption activation energy of O_2 on the catalyst surface is much smaller than that of CH_4, and O_2 is preferentially adsorbed on the catalyst surface to form adsorbed oxygen. Meanwhile, adsorbed oxygen species are easier to combine with adsorbed CH_4 than O_2 due to their electrophilic attack on CH_4, so that the hydrogen in CH_4 is dissociated, destroying the stable structure of CH_4 and generating active methyl radicals to promote the oxidation of CH_4. The L–H mechanism is mainly found on noble metals and their supported oxide systems (Becker et al., 2011). Trimm *et al.* studied methane oxidation over the Pt/Al_2O_3 porous catalyst and found that the rate equation derived by experimental results was best fit with the L–H mechanism (Trimm and Lam, 1980).

E–R mechanism. In the E–R mechanism, the gaseous O_2 is first adsorbed on the metal atoms of TMOs and then further activated to form surface-adsorbed oxygen, which reacts with

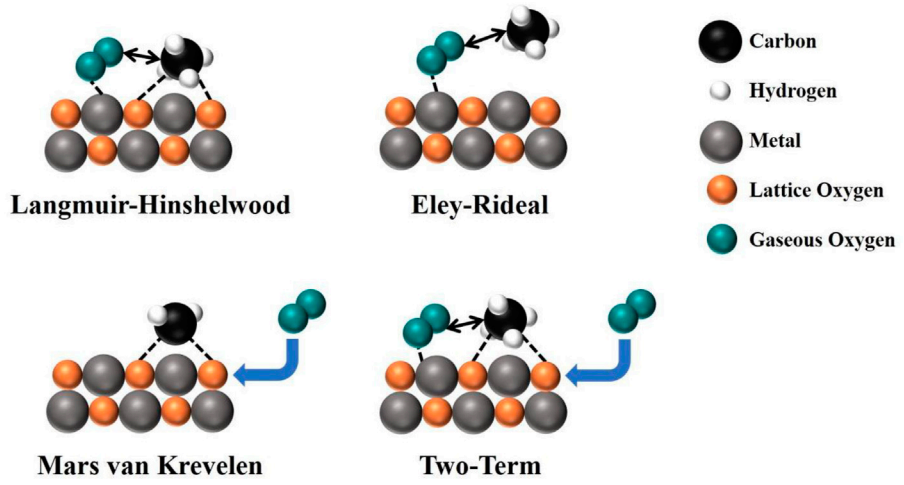

FIGURE 2
The reaction mechanism diagram of CMC.

gaseous CH_4 to form active methyl species, finally oxidized to CO_2 (Belessi et al., 2001). Veldsink *et al.* investigated the reaction rate of CMC over a commercially available CuO-γ-$A1_2O_3$ catalyst and derived a kinetic rate equation from all experimental data. The rate equation is in good accordance with the E–R mechanism, in which catalyst with adsorption of O_2, CO_2, and H_2O, but does not adsorb CH_4 (Veldsink et al., 1995).

MvK mechanism. MvK is a redox mechanism where the catalyst will be reduced by CH_4 at first, and then the active centers will be reoxidized by molecular oxygen uptakes. It includes surface oxygen reaction and lattice oxygen migration, in which the reaction pathway can be divided into the following steps: the surface dissociative adsorption of gaseous CH_4 onto the active site of the catalyst to form adsorbed alkyl and hydroxyl groups, and the reaction spills over to form CO_2 and H_2O products taking the lattice oxygen as the oxidizing source. After product desorption, the active centers will be reduced with a lot of formation of lattice oxygen vacancies, which can be replenished by either lattice oxygen diffusion from the bulk phase or molecular oxygen adsorption from the gas phase. This reaction mechanism is found for several TMOs like Fe_2O_3 and Co_3O_4 (Zasada et al., 2017; He L. et al., 2020).

T-T mechanism. Due to the complex nature of CMC, there are some cases where describing the reaction process on the catalyst by a single mechanism is rather challenging, and then the T-T mechanism is proposed, that is, both surface adsorption oxygen and lattice oxygen participate in the reaction simultaneously (Han et al., 2008). Gaseous oxygen adsorbs on metal active sites and then dissociates to form surface-active oxygen species. It oxidizes CH_4 together with lattice oxygen species that migrate from the bulk to the surface, and the lattice oxygen vacancies will be replenished by gaseous oxygen, resulting in some more suitable explanation of reaction mechanisms in CMC over TMOs (Wang et al., 2018).

Although in some cases that an explicit reaction model can be interpreted to well describe the reaction kinetics of TMO-catalyzed CMC reactions, such as Fe_2O_3, Co_3O_4, etc., the reaction mechanism may vary based on the structure of TMOs or the reaction conditions. For example, Zasada *et al.* systematically examined CMC over Co_3O_4 nanocubes, revealing that the content of oxygen vacancies significantly affects the reaction mechanism. In the low-temperature range (300–450°C), CH_4 is primarily activated by monatomic oxygen species on the catalyst, in which facile decarboxylation and dehydroxylation leave the catalyst surface stoichiometric, thus following the L–H mechanism. From 450 to 650°C, the intrafacial dehydroxylation and decarboxylation of the catalyst accelerated the formation of oxygen vacancies, making the catalyst surface slightly reduced. Then, oxygen vacancies are virtually refilled by O_2, which is in accordance with the coexistence of L–H and MvK mechanisms. Above 650°C, oxygen vacancies formed from the bulk Co_3O_4, so causing the active involvement of the lattice oxygen following the MvK mechanism. In this case, the varying reaction conditions change the catalyst redox states, in which the number of oxygen vacancies leads to a variety of reaction mechanisms (Zasada et al., 2017).

The mechanism of CMC may also be significantly altered by doping or substitution of other transition metal ions with different contents into transition metal oxides. Wang *et al.* demonstrated that the catalytic behavior can be regulated through the substitution of Co by Ni in spinel $ZnNi_xCo_{2-x}O_4$ oxides (Figure 3). In addition, the difference of catalytic behavior can be explained by the interaction between the O *p*-band center and metal *d*-band center. When the metal

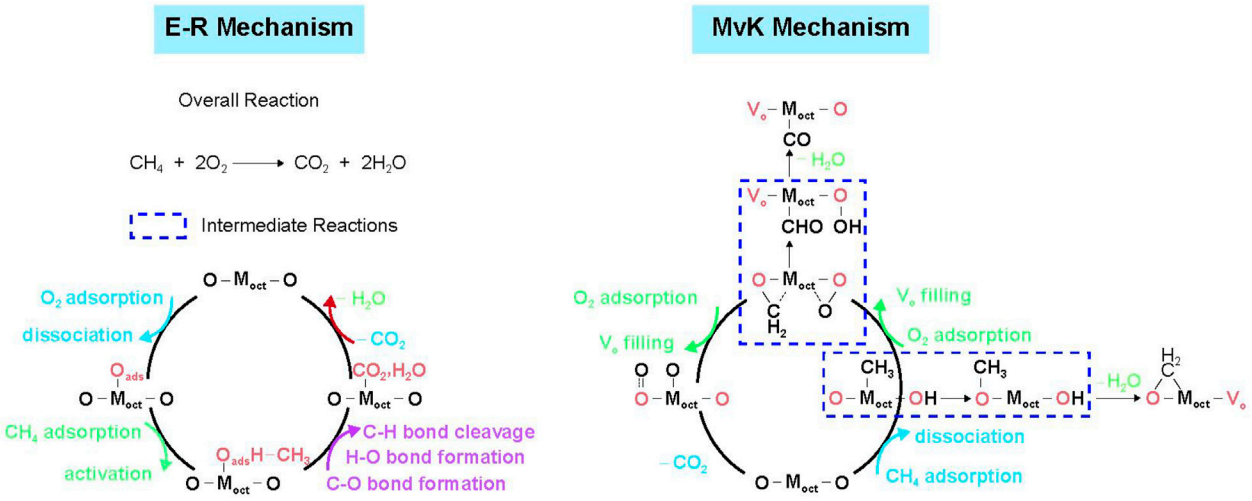

FIGURE 3
The proposed reaction pathways based on the E–R mechanism for Ni-poor spinel oxides and MvK mechanism for Ni-rich spinel oxides. Cited from Wang H. W. et al. (2019).

d-band center exhibits a higher position relative to the O *p*-band center in Ni-poor $ZnNi_xCo_{2-x}O_4$ spinel oxides, the catalyst shows a greater metal character, following the E–R mechanism, among which the first C–H bond cleavage and the H_2O desorption are considered to be the rate-determining steps. On the contrary, Ni-rich spinel oxides with the higher O *p*-band center compared with the metal *d*-band center show greater oxygen character, in accordance with the MvK mechanism, in which the multiple lattice oxygen involved steps are crucial for the entire methane oxidation (Wang T. et al., 2019).

The mechanism of CMC may also be greatly affected by the reaction temperature. He *et al.* investigated CMC over α-Fe_2O_3 *via* a combined experimental and theoretical study and found that $C^{16}O_2$ formed first, followed by $H_2{}^{16}O$, $C^{16,18}O_2$, $H_2{}^{18}O$, and finally $C^{18}O_2$, where $^{18}O_2$ was only used in the gaseous molecular oxygen. The numerical analysis of the mass balance revealed that the ratio $^{16}O/^{18}O > 1$ at T < 385°C, then $^{16}O/^{18}O \approx 1$ at T ≈ 385°C, and finally $^{16}O/^{18}O < 1$ at T > 385°C. These indicate that, below 385°C, the lattice oxygen plays a predominant active role in CMC reaction, in accordance with the MvK mechanism. However, above 385°C, the mechanism becomes more complex and difficult to analyze (He Y. L. et al., 2020).

3 Transition metal oxides for catalytic CH_4 combustion

In the application of the CMC, the TMOs such as Co_3O_4, NiO, MnO_2, Cr_2O_3, Fe_2O_3, CeO_2, CuO, and their binary complex oxides have been widely studied. Therefore, the characteristics of these TMOs and the mechanisms of the CMC over these catalysts are comprehensively reviewed in the following sections in order to provide a general guideline about the construction of well-performed catalytic systems for the CMC. The catalytic performances of different TMOs for CMC are shown in Table 1.

3.1 Co_3O_4-based catalysts

3.1.1 Single Co_3O_4

Co_3O_4 is a p-type semiconducting metal oxide with a typical spinel structure, and it has an array based on a cubic close-packed oxide ion whose lattice parameter is a = 0.811 nm with the space group of Fd3m. In the crystal structure of Co_3O_4, Co^{2+} occupies the tetrahedral coordination and Co^{3+} occupies the octahedral coordination, respectively, with a mean cobalt oxidation state of +2.67. Co_3O_4 is considered to be one of the most effective co-oxidation catalysts due to the unfilled 3*d* orbital of Co, the weak Co–O bond strength, a high cycle frequency of redox, and a low barrier of oxygen vacancy. Owing to its unique physical and chemical properties, it has a wide range of applications in sensors, magnetic materials, lithium-ion batteries, and solar cells (Sanchis et al., 2021). In CMC, Co_3O_4 has attracted the attention of many researchers due to its high stability, variable valence, and excellent catalytic performance. Paredes *et al.* found the activity of different bulk TMOs catalysts in methane combustion in the following order: Co_3O_4 > Mn_2O_3> Cr_2O_3> CuO > NiO (Paredes et al., 2009). Therefore, Co_3O_4 is considered to be one of the best candidates for CH_4 combustion catalysts

TABLE 1 The catalytic performances of different TMOs for CMC.

TMOs	Preparation method	Surface area (m^2 g^{-1})	Light-off temperature (°C)	E_a (kJ mol^{-1})	Feed composition and GHSV/WHSV (gas/weight hourly space velocity)	Stability	Reaction mechanism	References
Co_3O_4	basic precipitation	14	T_{50} = 330	74 ± 2	1% CH_4, 10% O_2 and 89% N_2 GHSV: 60,000 h^{-1}	anti-H_2O: good (reversible deactivation) anti-SO_2: none	MvK	Choya et al. (2022)
Co-In-0.2 oxide	a designed precipitation	57.3	T_{10} = 265 T_{99} = 395	82.2	1% CH_4, 10% O_2, N_2 (balance); GHSV = 48,000 ml g^{-1} h^{-1}	anti-H_2O: excellent (fully restored) anti-SO_2:: none	none	Zheng Y. et al. (2020)
N-Co_3O_4-110	a facial N_2 plasma engraving	52.3	T_{50} = 342 T_{90} = 412	73.0	2 vol. % CH_4, 20 vol. % O_2, 5 vol. % H_2O, Ar gas; WHSV = 46,800 ml g^{-1} h^{-1}	anti-H_2O: good (reduced by about 3%) anti-SO_2:: none	May be MvK	Yu et al. (2020)
$Co_3O_4/Ce_{0.75}Zr_{0.25}$	solution combustion synthesis	none	T_{50} = 217 (with electric field)	35.8 (with electric field)	[CH_4] = 0.2%, [O_2] = 10%, N_2 (balance gas); GHSV = 30,000 h^{-1}	none	MvK	Li K. et al. (2019)
Mesoporous Co_3O_4	Calcining	136.2	T_{10} = 220 T_{50} = 270	none	1% CH_4, 20% O_2; space velocity = 18,000 ml g^{-1} h^{-1}	none	E-R	Han et al. (2016)
Zr-Doped NiO	homogeneous co-precipitation strategy	142	T_{90} = 380	55.27	1 vol% CH_4, 10 vol% O_2, balanced N_2 GHSV: 30,000 ml g^{-1} h^{-1}	anti-H_2O: good anti-SO_2: none	MvK	Wang et al. (2021)
Ni-Cu mixed oxides	co-precipitation method	147	T_{50} = 370 T_{90} = 410	89	1 vol% CH_4, 5 vol% O_2 and N_2 GHSV: 50 000 ml g^{-1} h^{-1}	anti-H_2O: good anti-SO_2: none	MvK	Fan et al. (2022)
Mn-Ce-RP	redox-precipitation method	none	T_{50} = 446°C	none	CH_4(1%)/O_2(10%)/N_2 WSHV = 30,000 ml/(g*h)	anti-SO_2: excellent anti-H_2O: none	MvK	Zhong et al. (2019)
nanocubic MnO_2	a hydrothermal process	78	T_{50} = 293 T_{90} = 350	none	none	none	L- H	Zhang et al. (2019)
α-MnO_2	a hydrothermal	92.9	T_{50} = 356 T_{90} = 463	none	0.1% CH_4 in air WHSV = 90 L g^{-1} h^{-1}	none	MvK	Jia et al. (2019)
MnO_2/ZrO_2	one-pot hydrothermal	none	T_{50} = 340	none	1,000 ppm CH_4, 10% O_2, and N_2 (balance) WHSV = 45 L g^{-1} h^{-1}	anti-H_2O: good anti-SO_2: good	none	Jia et al. (2018)
Nano-$ZnCr_2O_4$ spinel oxides	a ethylene glycol-mediated solvothermal	96.2	T_{10} = 300 T_{90} = 400	144.8	2 vol% CH_4, 20 vol% O_2, 78 vol% N_2 GHSV = 78,000 h^{-1}	none	L-H	Huang et al. (2019)
Sn-Cr binary oxide	a co-current co-precipitation	133	T_{10} = 320 T_{50} = 400 T_{90} = 490	none	1.0% CH_4 in air; space velocity = 20,000 h^{-1}	none	MvK	Zhu et al. (2003)
Fe and Cr-based oxides $Fe_{60}Cr_{40}$	the citrate sol–gel	82	T_{450}°C = 79% T_{550}°C = 97%	none	347 ppm CH_4+5.1 ppm SO_2	anti-H_2O: good anti-SO_2: excellent	none	García-Vázquez et al. (2020)
Bulk α-Fe_2O_3	precipitation	none	T_{50} = 461	99.9	2000 ppm V CH_4 in air	none	MvK (100–500°C)	Paredes et al. (2004)
Nano sheetα-Fe_2O_3	hard-templating	none	T_{10} = 230 T_{50} = 394	17.60	5% CH_4 and 20% O_2 balanced with 75% Ar; WHSV = 10 000 ml g^{-1} h^{-1}	none	MvK (below 400°C)	He Y. L. et al. (2020)

(Continued on following page)

TABLE 1 (*Continued*) The catalytic performances of different TMOs for CMC.

TMOs	Preparation method	Surface area (m^2 g^{-1})	Light-off temperature (°C)	E_a (kJ mol^{-1})	Feed composition and GHSV/WHSV (gas/weight hourly space velocity)	Stability	Reaction mechanism	References
NiO/CeO_2	Deposition precipitation	none	T_{50} = 465	69.4 ± 4.0	20 ml/min 10% CH_4/Ar and 10 ml/min pure O_2 WHSV = 18 000 ml g^{-1} h^{-1}	anti-H_2O: good anti-SO_2: none	MvK	Zhang et al. (2018)
$MnCeO_x$ (Mn-to-Ce ratio of 1:3)	redox	none	T_{50} = 475 T_{100} = 700	113	CH_4/O_2/He mixture (concentration: 1/4/95); Space velocity = 30,000 h^{-1}	none	MvK	Palella et al. (2021)
$Ce_{0.9}Zr_{0.06}Sc_{0.04}O_{1.98}$	citrate complexation	none	T_{50} = 700	124.3	1 vol% CH_4, 8 vol% O_2 and 91 vol% N_2	none	MvK	Toscani et al. (2019)

among all TMOs and a promising alternative for noble metal combustion catalysts.

According to the previous literature, the common methods for preparing Co_3O_4 include precipitation, sol–gel method, hydrothermal synthesis, impregnation, thermal decomposition, and solid phase reaction. Choya *et al.* prepared several bulk Co_3O_4 catalysts by various synthesis methodologies, among which the solution combustion synthesis route, the basic grinding route, the calcination of the cobalt hydroxycarbonate route, and the precipitation with the sodium carbonate route showed better textural properties than the commercial catalyst due to the higher presence of Co^{3+} on their surface and further resulted in abundant lattice oxygen species. The catalysts exhibited higher catalytic activities due to their favored mobility of lattice oxygen species (Choya et al., 2022). Wang *et al.* prepared a series of Co_3O_4/γ-Al_2O_3 catalysts by a combination of incipient wetness impregnation (IWI) and subsequent combustion synthesis (CS) method. Results revealed that the CS method exhibited higher catalytic activity than the catalysts prepared by the IWI method, attributing to the higher surface area, lower Co_3O_4 crystallization, better dispersion, more surface Co^{3+}, as well as easier and faster redox cycle between Co^{2+} and Co^{3+} (Wang et al., 2015).

Studies have shown that the catalytic behavior of Co_3O_4 catalysts strongly depends on its morphology, structure, and crystal planes, which endow them with different electron transfer abilities and different amounts of active sites, promoting catalytic activity and selectivity. The morphological characteristics can be regulated by the preparation method, such as spheres, nanorods, nanowires, nanobelts, and nanosheets.

Wang *et al.* prepared Co_3O_4 with the shape of nanosheets and nanospheres by the hydrothermal method in media of ethylene glycol and water, respectively. The concentration of ethylene glycol and the hydrothermal temperature significantly influenced the size and shape of the Co_3O_4, which showed that the Co_3O_4 nanosheets exhibited slightly higher catalytic performance than the Co_3O_4 nanoparticle, as more active oxygen species were found in the former (Wang et al., 2017). Chen *et al.* controllably synthesized Co_3O_4 nanocrystals with different morphologies (flower, hexagonal plate, hexagonal sheet, and cube), which showed that the properties of Co_3O_4 were closely related to the morphology. Compared to cubical Co_3O_4 with the (100) plane, the flower-like, hexagonal plate-like, and hexagonal sheet-like Co_3O_4 catalysts were more active, which may be due to more exposed (111) planes (Chen et al., 2016).

In addition, the spatial structures of TMOs also play an important role in the catalytic activity. Sun *et al.* prepared Co_3O_4 catalysts with different spatial structures, such as 0D (nanoparticles), 1D (nanorods), 2D (nanoplates), and 3D (mesoporous and microporous) structures. Among them, 2D structures (nanoplates) have the best catalytic activity, which is contributed to the high refractive index of the exposed (112) crystal planes and the role of surface-active species (such as surface-adsorbed oxygen and Co^{2+}) in the catalytic reaction (Sun et al., 2016).

The use of supports can effectively improve the dispersion and prevent the particle agglomeration caused by the sintering of the Co_3O_4 catalyst, thereby improving the catalytic activity of the catalyst. Feng *et al.* deposited Co_3O_4 on the $SmMn_2O_5$ (SMO) support to prepare Co/SMO composite catalysts and evaluated the performance of Co/SMO catalysts in oxygen-enriched environments. The results showed that the Co/SMO-50% catalyst had high catalytic activity and strong durability. The strong interaction between Co_3O_4 and $SmMn_2O_5$ played a key

role in dispersing and stabilizing Co_3O_4 by preventing catalyst sintering. Highly dispersed Co_3O_4 formed more surface lattice oxygen-oxidized CH_4, leading to the transformation from Co^{3+} to Co^{2+}, along with the formation of an oxygen vacancy, which could be compensated by the gaseous oxygen, so following the MvK mechanism (Feng et al., 2018). Dou *et al.* obtained Co_3O_4/CeO_2 catalysts by supporting Co_3O_4 nanoparticles on CeO_2 nanorods by the deposition precipitation method. The results showed that complete oxidation of CH_4 on Co_3O_4/CeO_2 (43.9 kJ/mol) was obviously lower than pure CeO_2 (95.1 kJ/mol) and pure Co_3O_4 (89.7 kJ/mol). Co_3O_4/CeO_2 showed synergistic effect, in which oxygen vacancies on the surface of CeO_2 were active centers for activating molecular oxygen in the oxidation reaction, thus promoting the improvement of catalytic activity (Dou et al., 2018).

3.1.2 Doped Co_3O_4

The element doping has been considered as an effective way to adjust the surface and electronic structures of nanomaterials. Some studies show that introducing oxygen vacancies will have a huge effect on the oxidation reaction. In the element-doped catalyst, Co_3O_4, as the reactive site, actively participates in CMC, while the doping of other elements often creates more oxygen vacancies to promote the rapid migration of lattice oxygen (Rodríguez-Fernández et al., 2019). Zheng *et al.* believed that Co^{2+} was active species in Co_3O_4. Thus, they prepared Co-In-x oxide *via* a designed precipitation method by taking N-butylamine as the precipitant. The Co–In–O solid solution phase exhibited a superior activity by doping an appropriate amount of In^{3+} to replace the Co^{3+} site of octahedral position, increasing the proportion of active species Co^{2+}, giving rise to abundant active oxygen species, improving reducibility, and optimizing surface acidity. Moreover, Co–In-x oxide also demonstrated excellent stability and water resistance, indicating that the doping of In^{3+} was beneficial to maintain a certain grain size and crystal phase (Zheng Y. F. et al., 2020). Yu *et al.* prepared the defective N-doped Co_3O_4 by efficient N_2 plasma treatment for methane oxidation reaction. N-doped Co_3O_4 could synergistically boost the catalytic performance by increasing active surface oxygen, enhancing redox property, and promoting the C–H bond activation ability. This result may provide a valuable guidance for the defects engineering of Co_3O_4 for the application of CMC (Yu et al., 2020).

However, doping is not always favorable for the catalytic activity of Co_3O_4. Choya *et al.* prepared two bulk Co_3O_4 catalysts with and without residual sodium by precipitation method. It was found that the presence of Na^+ had a negative impact on the properties of the Co_3O_4 catalyst due to diffusion and migration into the spinel lattice. The insertion of Na^+ led to lattice distortion and induced a reduction of the Co^{3+} into Co^{2+} owing to high Lewis acidic properties, along with high electron density within the oxygen ions of the lattice, weakened Co–O bonds, and reduced lattice oxygen species, which pointed out that the doping may be detrimental to catalytic performance. In this sense, appropriate precipitants or preparation methods are important for achieving high-performance CMC catalysts (Choya et al., 2018b).

3.1.3 Binary Co_3O_4-catalysts

Li *et al.* reported the introduction of an electric field on the Co_3O_4/$Ce_{0.75}Zr_{0.25}$ catalyst and found that the presence of the electric field significantly promoted the catalytic oxidation activity of methane. Co_3O_4 provided active sites and oxygen species for methane oxidation, while CeO_2 released lattice O species for the oxidation of CoO and Co to Co_3O_4. The electric field promoted the reduction of Ce^{4+} to Ce^{3+} and promoted the release of oxygen from the lattice. The chemisorption of methane mainly located in the newly formed tetrahedral Co^{3+} in the electric field rather than the active sites formed by octahedral Co^{3+} with gaseous oxygen. The adsorbed CH_4 was oxidized to carbonates species immediately, followed by the formation of CO_2 and refreshment of consumed O species by gaseous oxygen, which is similar to the typical MvK mechanism (Li L. et al., 2019).

3.1.4 Deactivation

Although Co_3O_4 shows a high catalytic activity for the CMC, it still cannot defeat noble metals owing to its low water and sulfur resistance. Generally, the inhibition of water vapor on the catalytic activity is probably due to its competition with the reactant for the active sites. The inhibition of SO_2 is attributed to the formation of sulfate or sulfide on the surface of catalysts, which may cause the loss of active sites, or agglomeration and the loss of surface area. From the existing literature, this problem can be effectively solved when the TMOs are supported on the carriers or some additives are added to the TMOs (Li J. A. et al., 2019).

Li *et al.* prepared a series of CoO_x embedded in the porous SiO_2 matrix by a spontaneous deposition method, which showed enhanced catalytic activity as compared with the simply supported CoO_x/SiO_2 catalyst due to a higher ratio of O_{ads}/O_{latt} and more active sites obtained by embedded CoO_x/SiO_2. Due to the competitive adsorption of water and reaction molecules on the active sites, water vapor inhibits the catalytic efficiency. While when H_2O was removed, the CH_4 conversion nearly fully recovered. Under moisture conditions, the embedded CoO_x@SiO_2 exhibited a high thermal stability and efficient moisture resistance due to the silica encapsulation (Li K. et al., 2019).

3.1.5 Mechanisms

According to the available mechanism study on CMC over TMOs, CMC over Co_3O_4 usually follows the MvK mechanism, which means that CH_4 is actually oxidized by the oxygen species present in the Co_3O_4 lattice, followed by the generation of oxygen vacancies. Then, the O_2 from the gas phase refills the oxygen

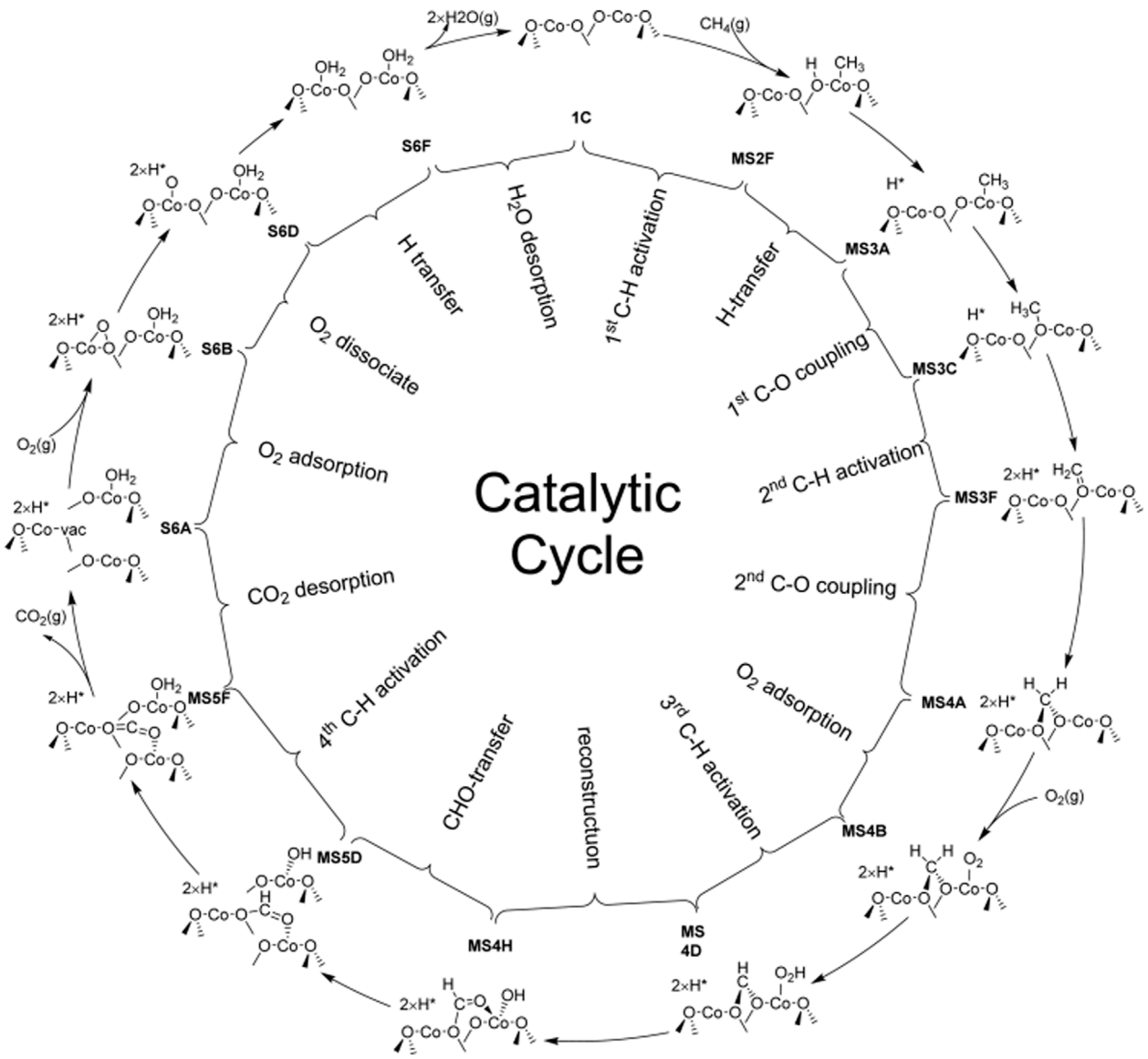

FIGURE 4
Schematic diagram of the whole catalytic cycle of CMC over Co_3O_4 (110) following the optimal reaction mechanism. Reprinted with permission from Hu et al. (2016). Copyright (2016) American Chemical Society.

vacancies, provoking the subsequent reoxidation of the Co_3O_4-basedcatalyst. Wu *et al.* prepared Co_3O_4–CeO_2 mixed oxides using $(NH_4)_2CO_3$, Na_2CO_3, and $CO(NH_2)_2$ as precipitation agents by a precipitation method. The Co_3O_4–CeO_2 with the homogeneous precipitation of $CO(NH_2)_2$ showed excellent catalytic activity owing to the small crystallite size, easy reducibility of Co^{3+}, and high surface Co^{3+} content at the Co_3O_4–CeO_2 interface. The peculiar structure and morphology of CeO_2 played a fundamental role in stabilizing the Co_3O_4 active phase against sintering and promoting its activity. The authors believed that the pathway of CMC over the Co_3O_4–CeO_2 was in accordance with the MvK mechanism, in which the Ce^{4+}/Ce^{3+} couple efficiently released oxygen (Wu et al., 2015).

Hu *et al.* investigated CMC on the Co_3O_4(110) surface with excellent catalytic performance by first-principles calculations as compared with that on the Co_3O_4(100) surface. It is found that the optimal reaction pathway of CMC over Co_3O_4(110) would be $CH_4 \rightarrow CH_3^* \rightarrow CH_3O_{2c} \rightarrow CH_2O_{2c} \rightarrow O_{2c}CH_2O_{2c} \rightarrow O_{2c}CHO_{2c} \rightarrow O_{2c}CHO^* \rightarrow CO_2$, in which the 2-fold coordinated lattice oxygen (O_{2c}) was the key to the first two C–H bond activations and the C–O bond coupling (Figure 4).

According to the figure, H is able to readily transfer swiftly among different surface oxygen species to form adsorbed H_2O^* for the rapid regeneration of active O_{2c}. The cooperation of multiple active sites not only facilitates the H swift transfer in order to maximally prevent the passivation of the active low-coordinated O_{2c} but also stabilizes surface intermediates during the CMC. Due to the synergistic effect of surface-adsorbed oxygen and lattice oxygen, the reaction pathway belongs to the T-T mechanism, in which the first C–H bond activation step would be the rate-determining step for the CMC on the Co_3O_4 (110) surface (Hu et al., 2016).

However, some researchers have proposed different mechanisms for the CMC over Co_3O_4. Han *et al.* prepared a series of Co_3O_4 nanocrystals with different morphologies *via* calcining the $Co(OH)_2$ precursor at different temperatures, among which the mesoporous Co_3O_4 possessed excellent catalytic activity due to the vacancy, antisite, dislocation, and grain boundary defects in the narrow junction regions and the structure of the pore wall. The authors believed that the reaction pathway followed the E–R mechanism, however, without detailed verification (Han et al., 2016).

3.2 NiO-based catalysts

3.2.1 Single NiO

NiO, NaCl-type cubic spar structure, is a typical P-type semiconductor with the intrinsic defects at the Ni^{2+} metal sites, which give rise to positive holes (p^+) to generate Ni^{3+} ($Ni^{2+} + p^+ \rightarrow Ni^{3+}$) or O^- species ($O^{2-} + p^+ \rightarrow O^-$). NiO is extensively used in the field of catalysis, chemical sensors, battery electrodes, and magnetic and electronic devices due to excellent properties such as catalytic activity, thermo-sensitivity, and super-paramagnetic property (Wang et al., 2021). Especially, in the field of catalysis, NiO-based catalysts attract a lot of attention due to the surface electrophilic O^{2-} species being effective for the activation of C–H bonds. NiO have been successfully prepared *via* a variety of methods, including chemical precipitation, electrode deposition, sol–gel technique, surfactant-template, hydrothermal technique, template-free strategy, microwave-assisted gas/liquid interfacial method, and solvothermal method.

Ye *et al.* prepared polymorphous NiO with different morphologies, including nanoparticle-based sheets, octahedra, nanosheet-built agglomerates, and nanoparticle-based microsphere, *via* a simple one-pot thermal decomposition approach. The morphology and crystal properties of NiO can conveniently be achieved by selecting various decomposition temperatures and precursors. The nanoparticle-based sheets and nanosheet-built agglomerates showed a high catalytic performance owing to the small crystal size and large specific surface area by using $NiC_2O_4{\cdot}2H_2O$ and $NiCO_3{\cdot}2Ni(OH)_2{\cdot}4H_2O$ as precursors (Ye et al., 2016).

Chen *et al.* prepared NiO-NSL nanomaterials with a characteristic nanorod structure through the solid–liquid $NH_3{\cdot}H_2O$ precipitation method. The content of Ni^{2+} on the surface of NiO-NSL was higher than traditional NiO-based catalysts, consistent with DFT calculations in which the energy barrier for the C–H bond activation on Ni^{2+} was lower than that on Ni^{3+}. However, the authors did not clearly explain the mechanism of the CMC on the NiO-NSL catalyst, but only highlighted the significant impact of Ni^{2+} on the catalytic performance of the NiO-based catalysts (Chen K. et al., 2021).

3.2.2 Doped NiO

Generally, the synergistic effect induced by the doping can significantly improve catalytic activity. Zhang *et al.* prepared a series of MnO_x–NiO composite oxide catalysts by the co-precipitation method, which exhibits higher catalytic performance compared with the single NiO and MnO_x. The characterization results demonstrate that the Ni–Mn–O solid solution formed by the doping of appropriate amount of Mn, showing abundant highly dispersed Mn^{4+} and higher coordination number as well as certain nickel vacancies, due to the synergy interaction of Ni and Mn (Zhang et al., 2013).

3.2.3 Binary NiO-catalysts

Fan *et al.* introduced Cu into the NiO lattice to generate the Cu–Ni solid solution with the mesoporous structure by the co-precipitation method. Ni–Cu oxide catalysts manifested superior catalytic activity, moisture tolerance, and durability, owing to more unsaturated Ni atoms and lattice defects. Ni–O–Cu bonds could weaken Ni–O and Cu–O bonds, making the lattice oxygen converted into adsorbed oxygen efficiently and creating more oxygen vacancies to promote the activation and adsorption capacity of Ni–Cu oxide for O_2, creating more surface electrophilic species (O_2^{2-}, O_2^- and O^-). Thus, the reaction pathway was in agreement with the MvK mechanism (Figure 5). The electron densities were redistributed because of the interaction between NiO and CuO, where the surface acid–base properties were adjusted. The higher basicity over Cu–Ni oxide could contribute to the adsorption of CH_4 with weak acidity and inhibit the accumulation of surface hydroxyl groups effectively. Meanwhile, the stronger surface acid sites could facilitate the activation of CH_4 *via* heterolytic C–H bond breaking (Fan et al., 2022).

3.2.4 Deactivation

Through the regulation of preparation method and structure, Ni-based catalysts can obtain excellent resistance to water vapor. Liu *et al.* prepared the simple metal oxides (Fe_2O_3, Co_3O_4, NiO, and CuO) by the thermal decomposition of the corresponding metal nitrates. The NiO possessed larger capability for oxygen adsorption, thus exhibiting the best catalytic activity for CMC as compared to other metal oxides, even superior to the perovskite catalyst $LaCoO_3$. Water vapor promoted CH_4 conversion over the

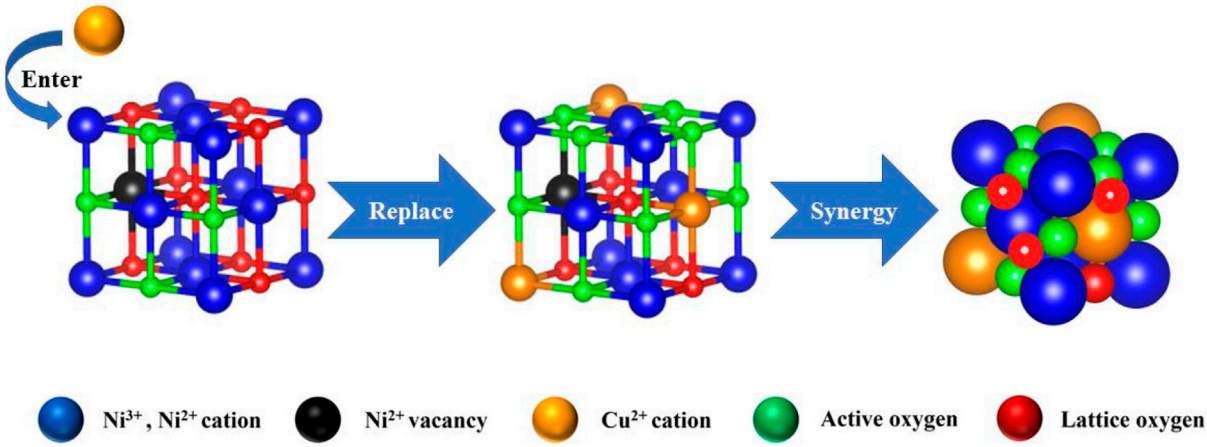

FIGURE 5
Reaction pathway of CMC over Cu–Ni oxide. Cited from Fan et al. (2022).

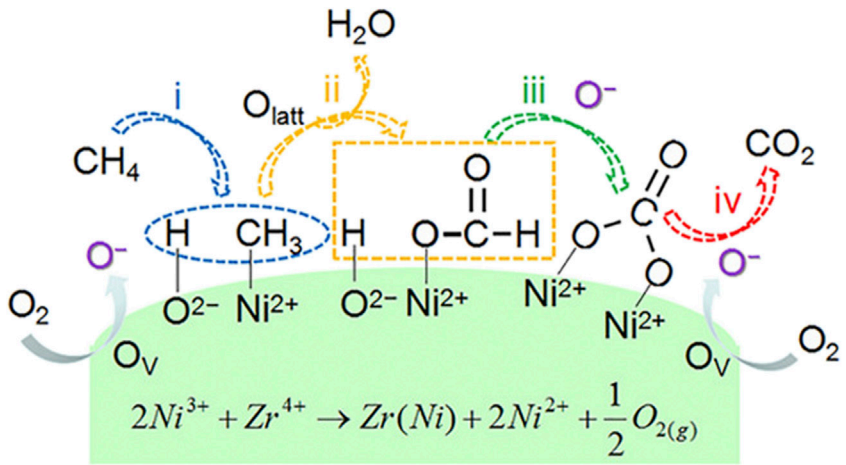

FIGURE 6
Reaction pathway for methane combustion over $Ni_{1-x}Zr_xO_{2-\delta}$ catalysts. Reprinted with permission from Wang et al. (2021). Copyright (2021) American Chemical Society.

NiO catalyst, which could be attributed to H_2O could modify NiO surface and promote the activation of O_2 and CH_4 on the surface (Liu et al., 2017). Xu *et al.* synthesized NiO catalysts with the mesoporous structure by hydrothermal method with polyethylene glycol (NiO-PEG) and polyvinyl pyrrolidone (NiO-PVP) as soft templates. NiO-PEG and NiO-PVP possessed more mobile-active oxygen species, which was beneficial to the activating of the CH_4, due to the mesoporous structure and high surface area. NiO-PEG displayed excellent reaction stability in the presence or absence of water vapor for the reason that its bulk structure possessed certain physical stability (Xu et al., 2017).

3.2.5 Mechanisms

It is generally believed that the pathway of the CMC over nickel-based catalysts is consistent with the MvK mechanism. Shu *et al.* prepared mesoporous NiO with abundant oxygen defects by a NaCl crystalline scaffold-based method. In kinetic measurements, r_{CH4} exhibited a near zero-order dependence on O_2 partial pressure, indicating that CH_4 oxidation was not sensitive to the P_{O2} partial pressure. Due to the depletion of lattice oxygen, the concentrations of $C^{16}O^{16}O$ and $C^{18}O^{16}O$ were reduced, and the concentration of $C^{18}O^{18}O$ was increased, which further demonstrated that the reaction mechanism was accorded

with the MvK mechanism. In this case, the highly abundant lattice oxygen species had great contribution to the excellent performance of NiO (Shu et al., 2022). Wang *et al.* prepared Zr-promoted NiO nanocatalysts by a designed co-precipitation process. $Ni_{0.89}Zr_{0.11}O_{2-\delta}$ solid solution phase exhibited abundant active Ni^{2+} sites and oxygen vacancies, bringing about the increase in surface acidic–basic sites. The mechanism for CMC could be described, as shown in Figure 6. CH_4 was adsorbed on the Ni^{2+}–O^{2-} active site at first and then dissociated to -CH_3 and -OH, followed by the formation of formate and carbonate intermediates. Then, the carbonate species converted to CO_2. The authors did not mention which mechanism the CMC on $Ni_{0.89}Zr_{0.11}O_{2-\delta}$ conforms to, but according to the lattice oxygen and oxygen vacancies involved in the reaction, it is judged that the reaction conforms to the MvK mechanism. Meanwhile, in the stream tests, the steady conversion of CH_4 could be well maintained regardless of the presence of H_2O due on the doping of Zr (Wang et al., 2021).

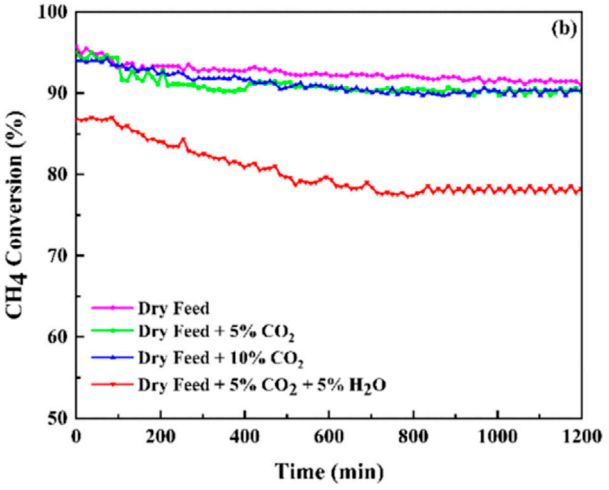

FIGURE 7
Catalytic stability for methane catalytic combustion of the MnO_2 catalyst under different feed compositions. Reprinted with permission from Akbari et al. (2021). Copyright (2021) American Chemical Society.

3.3 MnO_2-based catalysts

3.3.1 Single MnO_2

Mn oxides, such as α- and β-MnO_x, possess the different polymorphic structures, which exhibit mixed valence state of Mn (Mn^{2+}, Mn^{3+}, and Mn^{4+}), and different ways to link together the basic octahedral [MnO_6] units, thereby showing strikingly different and efficient catalytic activities for the CMC (Jia J. B. et al., 2016; Yang et al., 2021). The catalytic activity of the Mn oxides is typically determined by their prepare method, morphology, crystal structure, and degree of oxidation.

Yu *et al.* prepared γ-MnO_2 with abundant surface and lattice defects by a combined ball-milling and selective atom removal method, which showed a high catalytic activity for the CMC owing to the enhanced specific surface area, high Mn^{4+}/Mn^{3+} ratio, more active oxygen species, and enhanced reducibility (Yu et al., 2019). Wasalathanthri *et al.* prepared mesoporous amorphous Meso-Mn-A, Meso-Mn_2O_3, Meso-ε-MnO_2 (epsilon phase), and octahedral molecular sieves MnO_2 (Meso-OMS-2) *via* an inverse surfactant micelle method. Meso-OMS-2 showed the highest catalytic activity, attributing to the narrow and monomodal pore size distribution, higher surface area, the oxidation states, and surface oxygen vacancies, promoting the lattice oxygen mobility, following the MvK mechanism (Wasalathanthri et al., 2015).

3.3.2Doped MnO_2

In addition, compared to pure MnO_x, the doping of other transition metals will also significantly enhance the catalytic performance of Mn-based oxides. Neatu *et al.* studied CeO_2–MnO_x catalysts by three methods, illustrating that the CeO_2–MnO_x catalyst impregnated on the support surface showed superior catalytic activity as compared with the catalyst doped into the bulk. The authors believed that the CMC over the CeO_2–MnO_x catalyst was in accordance with the MvK mechanism, in which the oxidation of CH_4 took place using the lattice oxygen, consecutively with the reduction of Ce^{4+} and Mn^{4+} to Ce^{3+} and Mn^{3+}, respectively. The gaseous O_2 was used to reoxidize the surface to assure another catalytic cycle (Neatu et al., 2019).

3.3.3 Deactivation

However, water vapor will affect the catalytic activity of Mn-based catalysts for the CMC to some extent. Akbari *et al.* prepared nanostructured MnO_2 catalysts with various morphologies by the simple hydrothermal method and the solution method, among which the α-MnO_2 catalyst with a wire-like morphology exhibited the best performance for CMC. However, the stability of the optimal MnO_2 sample reduced to some extent with the water vapor in the reactant feed stream (Figure 7). On one hand, the coverage of the active sites by water vapor inhibited the adsorption of CH_4 and O_2 on the MnO_2 catalyst surface. On the other hand, the -OH group as an inert compound over lattice oxygen could also cause a decline in the catalytic stability (Akbari et al., 2021).

If in an oxidizing atmosphere, SO_2 will be oxidized to form sulfate, which will be deposited on the surface of MnO_2, hindering the multiple adsorption, activation, and oxidation of CH_4 over MnO_2, then causing the deterioration of catalytic activity. Zhong *et al.* synthesized MnCe-RP and MnCe-CP by the redox-precipitation (RP) and co-precipitation (CP) methods,

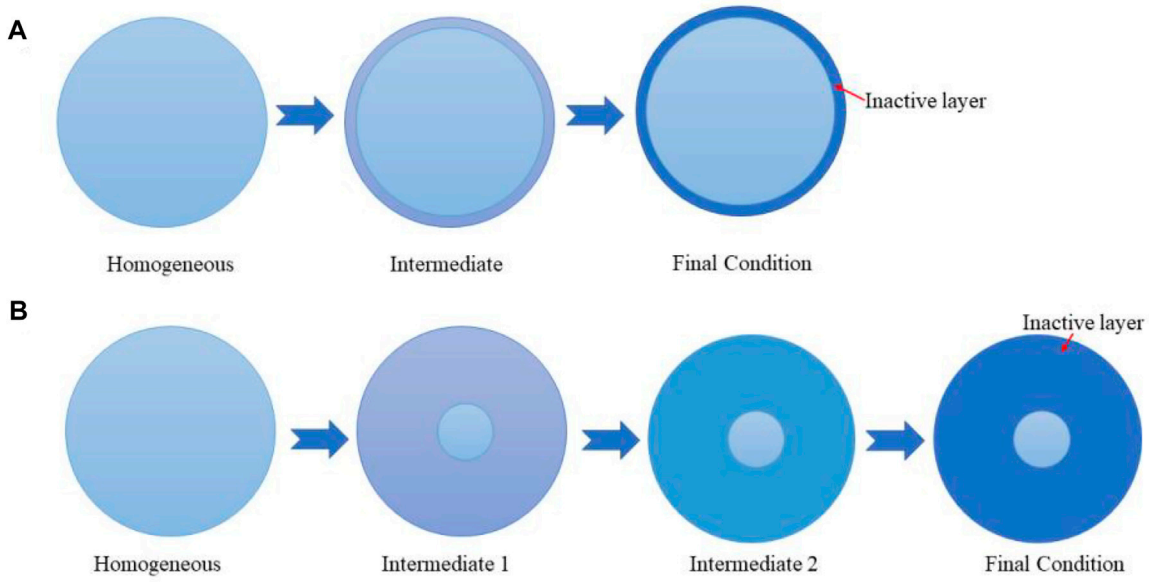

FIGURE 8
SO_2-poisoning mechanism over MnCe-CP **(A)** and MnCe-RP **(B)**. Cited from Zhong et al. (2019).

respectively, and studied SO_2 resistance of the catalysts (Figure 8). The SO_2 would decrease the content of lattice oxygen and Mn^{4+}, so the CH_4 conversion of MnCe-CP reduced by 62.45%. On the contrary, the CH_4 conversion of MnCe-RP only reduced by 1.08% owing to the excellent morphology and the redox potential of $K_xMn_8O_{16}$, absorbing and oxidizing SO_2 to sulfides, freeing from the poison of the downstream catalyst (Zhong et al., 2019).

3.3.4 Mechanisms

There are reported contradictory claims on the CMC over Mn oxides, such as that based on the L–H mechanism involving adsorbed oxygen and that based on the MvK mechanism concerning lattice oxygen.

Zhang *et al.* synthesized nanocubic MnO_2 (MnO_2-C) with planes (101) and nanorod-shaped MnO_2 (MnO_2-R) with planes (110) by a hydrothermal process, illustrating that the morphologies of MnO_2 had significant influence on the catalytic performances of CMC. Due to higher BET surface area, smaller crystalline size, more surface oxygen vacancies, and better low-temperature reducibility, MnO_2-C displayed higher catalytic performances and good thermal stability compared with MnO_2-R. The authors believed that the surface oxygen of MnO_2-C could react with the adsorbed C–H to generate the carboxylate species for the reason of more surface oxygen vacancies, followed by the oxidation of carboxylate species to CO_2, through the L–H mechanism (Zhang et al., 2019). Jia *et al.* synthesized two types of single-phase manganese oxides MnO_2 with different levels of nonstoichiometric defects, α-MnO_2 (Mn1) and γ-MnO_2 (Mn2), compared with a stoichiometric Mn_2O_3 (Mn3) as a reference. Results revealed that both Mn3 and Mn1 exhibited enhanced activities due to more structural defects. It was found that CH_4 was directly oxidized to carbonates on the surface of the pre-oxidized Mn1 and subsequently transformed to CO_2 in the absence of gaseous O_2 by the *in situ* DRIFTS and CH_4-TPD test, which showed that the active oxygen involved in the CH_4 oxidation was largely derived from the surface lattice oxygen of the Mn1, in accordance with the MvK mechanism. The O_2 on–off profiles further demonstrate reaction mechanism, in which the desorbed CO_2 was generated by the reaction between CH_4 and lattice oxygen from Mn1 without O_2, while the increase in CO_2 resulted from the reaction between CH_4 and the constantly refilled oxygen at the vacancies in the presence of O_2 (Jia et al., 2019).

Wang *et al.* studied the roles of the crystallographic structure of Mn-based oxides, among which α-MnO_2 exhibited the superior catalytic performances, attributing to higher surface Mn concentration and more active oxygen species, more mono-μ-oxo bridged (corner-shared) MnO_6 sites, and better reducibility. CMC over the MnO_2 catalyst proceeds *via* both MvK and L–H mechanisms, while the latter was predominant, in which the dehydrogenation of CH* to H* was considered as the rate-determining step and intermediate species -COO and -CH_3O were oxidized by active oxygen species to CO_2 and H_2O (Wang et al., 2018).

3.4 Cr_2O_3-based catalysts

3.4.1 Single Cr_2O_3

The Cr_2O_3, trigonal crystal system belongs to the α-Al_2O_3 structure, which is composed of oxygen ions as the closest hexagonal packing and Cr^{3+} filling the octahedral gap formed by these close packings. The coordination number of Cr^{3+} is 6, and only 2/3 of the octahedral gap is occupied by chromium ions. The activity and selectivity of Cr_2O_3 are closely related to the change of the valence state of chromium ions. Various techniques have been developed to prepare Cr_2O_3 nanoparticles such as co-precipitation, incipient wetness impregnation, sol–gel, solvothermal, solid thermal decomposition, and sonication (El-Sheikh et al., 2009).

Jodłowski *et al.* applied the sonication method to prepare transitional metal oxide catalysts (Co, Cu, Cr), among which the chromium oxide catalyst showed greater catalytic activity as compared to cobalt oxide, copper oxide, and commercial palladium catalysts, attributing to the presence of a high concentration of formate on the surface of chromium oxide (Jodłowski et al., 2016).

3.4.2 Doped Cr_2O_3

The doping of Cr_2O_3 enables the catalyst to exhibit excellent catalytic activity due to the synergistic effect between TMOs. Yuan *et al.* prepared Cr-based catalysts modified by Ce *via* incipient wetness impregnation method and investigated the effects of the Ce loading amount. It was found that the Cr-based catalysts with 3 wt% Ce showed higher catalytic performance due to an increasing amount of reaction site [CrO_4] species, improving the high-temperature-resistant performance and obtaining the synergistic effect between Ce and Cr (Yuan et al., 2013). Dupont *et al.* synthesized Cu/Cr oxides with high specific surface area by the sol–gel route using propionic acid. The results suggested that Cu/Cr oxides prepared by the special sol–gel process showed better catalytic performances compared with Cu/Cr oxide commercial catalysts, attributing to well-dispersed Cu species and the surface enrichment with Cr^{6+}. In addition, though DFT coupled with periodic slab models, the authors believed that O_2 molecules dissociatively adsorbed over the Cu/Cr oxide surface at the first step, along with generating the active oxygen species mainly at the Cr sites (Dupont et al., 2010).

3.4.3 Deactivation

Due to its poor affinity for acid gases, Cr_2O_3 exhibits excellent resistance to sulfur poisoning. Ordo´ñez *et al.* prepared different bulk metal oxides (Cr_2O_3, Co_3O_4, Mn_2O_3, NiO, and CuO) and investigated their catalytic stability for CMC in the presence of SO_2. It was found that Cr_2O_3 exhibited highly sulfur-tolerant, whereas the other materials were deactivated rapidly, even if Co_3O_4 and Mn_2O_3 were more active than Cr_2O_3 for CMC in the absence of sulfur species. Characterization results illustrated that the excellent stability was caused by the low affinity of Cr_2O_3 to acid gases (as SO_2); thus, sulfates would not form on the surface of the catalyst to occupy the active sites (Ordóñez et al., 2008).

3.4.4 Mechanisms

There is still controversy about the mechanism of CMC on Cr_2O_3. Huang *et al.* synthesized a homogeneous $ZnCr_2O_4$ oxides by the ethylene glycol-mediated solvothermal method. Cr^{3+} and Cr^{6+} coexisted in $ZnCr_2O_4$, in which Cr^{6+} probably caused the presence of interstitial oxygen species in the structure. The authors believed that the reaction pathway of CMC over the $ZnCr_2O_4$ catalyst was consistent with the L–H mechanism under low temperature, in which the interstitial oxygen was involved to the methane combustion. However, the mechanism has not been experimentally verified (Huang et al., 2019).

On the contrary, Zhu *et al.* applied the co-current co-precipitation method to prepare a series of Sn–Cr binary oxide catalysts among which the oxide with a Cr/Sn atomic ratio of 3 : 7 showed excellent catalytic activity due to higher surface areas and high oxidation states of chromium ions. Temperature-programmed ^{18}O isotope-exchange measurements confirmed that CMC over Sn–Cr binary oxide catalysts occurred *via* a redox cycle with the chromium ion as the active center, following the MvK mechanism (Zhu et al., 2003).

3.5 Fe_2O_3-based catalysts

3.5.1 Single Fe_2O_3

Fe_2O_3 is an earth-abundant and non-toxic material that has been extensively used to catalyze a wide range of reactions including water gas shift reaction, photocatalytic water splitting, looping combustion, etc. There are four polymorphs of Fe_2O_3, which are Hematite (α-Fe_2O_3), Maghemite (γ-Fe_2O_3), β-Fe_2O_3, and ε-Fe_2O_3. Among which α-Fe_2O_3 is thermodynamically stable and has the corundum(α-Al_2O_3) structure, which is based on a hcp anion packing. γ-Fe_2O_3 is an inverse spinel structure with cation-deficient sites and can be transformed from α-Fe_2O_3 at high temperature. β-Fe_2O_3 andε-Fe_2O_3 have been synthesized only in the laboratory. The former has been obtained by the de-hydroxylation of β-FOOH under high vacuum at 170°C. The structure of ε-Fe_2O_3 is intermediate between those of α-Fe_2O_3 and γ-Fe_2O_3. It can be prepared in various ways and transforms to α-Fe_2O_3 at between 500 and 750°C, apparently according to the method of preparation (Cornell and Schwertmann, 2003).

Among the few researches dealing with the use of Fe_2O_3 in CMC, α-Fe_2O_3 was the dominant catalytic active phase, and preparation method affects its catalytic performance greatly. Barbosa *et al.* synthesized bulk α-Fe_2O_3 by precipitation (α-Fe_2O_3-p) and the citrate method (α-Fe_2O_3-c), finding that the

preparation method strongly influences both the initial activity of the catalyst and its stability under reaction conditions (Barbosa et al., 2001). The α-Fe_2O_3-p catalyst presented higher surface areas, in correlation with greater initial activity and lower light-off temperatures than that of the α-Fe_2O_3-c catalyst. Although all catalysts undergo sintering at the high operation temperature with the loss of active sites, the α-Fe_2O_3-p catalyst exhibited less sintering and better stability. On this basis, Paredes *et al.* prepared α-Fe_2O_3 base catalysts *via* the acid dissolution-alkaline precipitation method using red mud as a raw material, an aluminum industrial waste formed by α-Fe_2O_3, Ti, Al, Ca, and Na, and compared the CMC performance and reaction mechanism with unprocessed red mud, and massive α-Fe_2O_3 synthesized by the precipitation method (α-Fe_2O_3-c mentioned above) (Paredes et al., 2004). For the combustion of 2000 ppm V CH_4 in air, the α-Fe_2O_3-c exhibits the best activity (T_{50} = 461°C), and the activity of processed red mud (T_{50} = 530°C) is much higher than that of unprocessed red mud (T_{50}>650°C) because after treatment the component of Na and Ca, which can hinder the catalyst activity decreases. Moreover, when conversion per Fe content in the catalyst is considered, the difference between α-Fe_2O_3-c and processed red mud catalysts is much smaller at low conversions. This would indicate that the other constituents of red mud have little or no effect on the catalyst activity. As for the mechanism, the CH_4-TPD experiments (100–600°C) suggested that very little CH_4 is adsorbed, the reticular oxygen of the catalyst being enough for its complete oxidation.

In addition, researchers have achieved the catalytic conversion of CH_4 over α-Fe_2O_3 catalysts with different morphologies. Dong *et al.* fabricated 3D urchin-like mesoporous α-Fe_2O_3 nanoarchitectures with the combination of nonhomogeneous ionic liquid/diphenyl ether solvothermal method and solid-state thermal annealing. They found that CH_4 was converted into products containing C–O bonds (CO_2) at 230°C, which is 190°C lower than over bulk α-Fe_2O_3. As for the reason, with the measurement and comparison of adsorbed oxygen on the two material, they inferred that the urchin-like α-Fe_2O_3 nanoarchitectures have a higher density of surface oxygen vacancies than bulk α-Fe_2O_3, which can accelerate the dissociation of oxygen molecules at the surface and increase the mobility of lattice oxygen (Dong et al., 2014). It should be noted that this structure does not exhibit good CH_4 conversion at high temperatures (700°C, conversion = 16%). He *et al.* invented a hard-templating synthetic strategy to guide the anisotropic growth of ultrathin α-Fe_2O_3 nanosheets with a large (110) facet exposure ratio, the catalytic performance of which in low-temperature CH_4 combustion is comparable to that of noble metal-based catalysts (He L. et al., 2020). The antiferromagnetic coupled diiron core on the (110) crystallographic plane of α-Fe_2O_3 is a structurally favorable condition, which resembles the diiron active site in soluble CH_4 monooxygenase, an enzyme that converts CH_4 to methanol in nature (Ross and Rosenzweig, 2017). Meanwhile, they utilized oxygen isotopic tracing experiments and DFT calculations to confirm that CH_4 is primarily activated by lattice oxygen below 400°C, in accordance with the MvK mechanism. They further speculated that at higher temperatures, CH_4 would be activated predominantly by molecular oxygen instead, as the accumulation of lattice oxygen vacancy favoring the adsorption of molecular oxygen from the gas phase (Cheng et al., 2016).

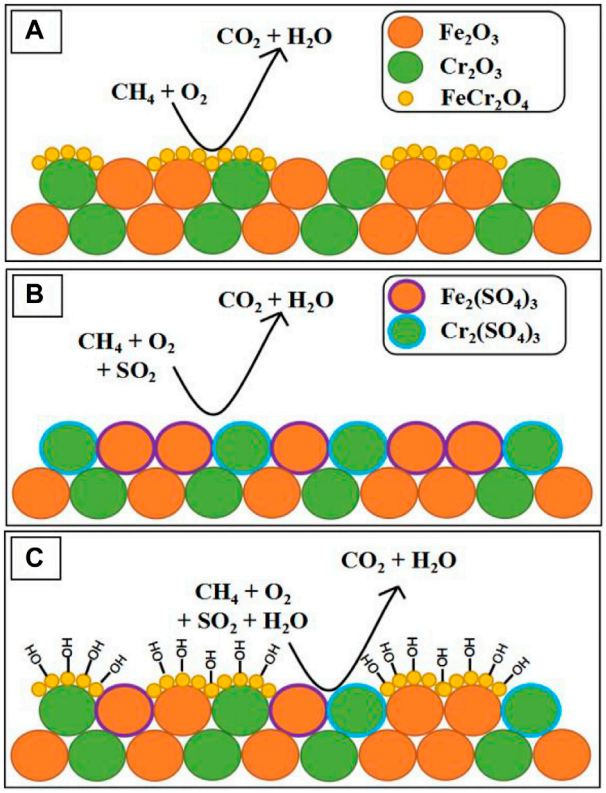

FIGURE 9
Proposed poisoning mechanisms at 450°C under **(A)** sulfur-free conditions, **(B)** dry conditions, and **(C)** wet conditions. Cited from García-Vázquez et al. (2020).

3.5.2 Deactivation

CH_4 emissions are often accompanied by large quantities of steam and traces of sulfur-containing gases, which are the two most performance hindering species present in typical CH_4 after-treatment operating conditions (Raj, 2016). Setiawan *et al.* confirm that α-Fe_2O_3 catalysts are significantly lower activity under the mixture conditions of water vapor and CH_4 due to the strongly bound between water (hydroxyl) species and Fe_2O_3, which destruct the active sites irreversibly (Setiawan et al., 2015). Recently, García-Vázquez *et al.* synthesized iron- and chromium-based oxides by using

the citrate sol–gel method and investigated their catalyst performance of CMC in the presence of SO_2 and steam. They found that catalyst $Fe_{60}Cr_{40}$ (molar ration) exhibited the remarkable performance (366 ppm CH_4 balanced in air, T = 450°C, conversion = 79%) due to the formation of the $FeCr_2O_4$ spinel phase, which is the most active sites in these catalyst for CMC. And because the $FeCr_2O_4$ spinel phase can still exits after being aged under wet conditions, the $Fe_{60}Cr_{40}$ showed the better catalyst conversion of CH_4 than α-Fe_2O_3 catalyst, which can also be found by comparing Figures 9A,B (312 ppm CH_4 + 4.6 ppm SO_2 10% vol H_2O balanced in air, T = 450°C, conversion = 47% vs. 26%). In addition, as has been represented in Figure 9C, the competitive adsorption of hydroxide groups on $FeCr_2O_4$ even slows down the rate at which sulfur dioxide poisons the catalyst's active sites (García-Vázquez et al., 2020).

3.5.3 Mechanisms

In conclusion, the reaction of α-Fe_2O_3 catalyst in CMC involves the MvK mechanism. Recently, Tang *et al.* adopted the generalized gradient approximation (GGA) + U approach to investigate the reaction pathways of complete and partial oxidations of CH_4 on the dominant Fe–O_3–Fe termination of thermodynamically stable hematite (α-Fe_2O_3) (0001) facets. The energy barrier for the first C–H bond activation is 1.04 eV. In the transition state, the dissociating H is in contact with the lattice O and with the dissociating CH_3 is in contact with the Fe site. Subsequent decomposition and oxidation of the CH_x species (x = 1, 2, 3) exploit the lattice O species according to the MvK mechanism, forming CH_xO in more thermodynamically and kinetically favorable pathways. For the two pathways, the overall rate-limiting steps are both the first C–H bond activation. Adsorption of O_2 on the VO site is exothermic (-1.42 eV), with one O atom binding at the VO site and the other O binding on the Fe site. In particular, after the dissociation of O_2 *via* the O–O bond cleavage, one O fills the oxygen vacancy, and the other O became the ferryl O (Fe=O). Although the ferryl O is highly active and capable of lowering the energy barrier of the C–H bond activation, the availability of extremely active ferryl O is expected to be too low on the Fe–O_3–Fe-terminated surface to critically impact the overall catalyst performance (Tang and Liu, 2016).

3.6CeO_2-based catalysts

3.6.1 Single CeO_2

CeO_2 is the most stable form of cerium oxide, which has a face-centered cubic structure and space group of Fm-3m (Trovarell, 2002). The coordination of cerium is 8 and that of oxygen is 4, which means that there are large vacant octahedral holes in the structure. Because of its structure, CeO_2 has an excellent storage-release capacity in a reversible manner. Specifically, Ce^{4+} can be reduced to Ce^{3+} under anoxic conditions, accompanied by a rapid release of lattice oxygen from the solid to the gas phase, leaving oxygen vacancy defects. On the other hand, Ce^{3+} can be re-oxidized into Ce^{4+} by adsorbing oxygen under oxygen-rich conditions and therefore refills the vacancies. Such unique redox properties render CeO_2 a wonderful support for noble metal catalysts in the catalytic oxidation of hydrocarbons, following mostly the MvK mechanism (Aneggi et al., 2016).

3.6.2 Doped CeO_2

CeO_2 has been actively studied in the past few decades as an alternative to noble metal catalysts for CMC (Mukherjee et al., 2016). While pure CeO_2 phase exhibits a poor catalytic activity at low temperatures and a poor thermal stability at high temperatures, which significantly hampers its industrial uses (Kašpar et al., 1999). Efforts have been made to improve the catalytic CH_4 combustion performance of CeO_2-based catalysts such as compositing with other metal oxides, heteroatom doping, etc. For instance, more oxygen vacancies can be introduced into the CeO_2 structure by doping cations with oxidation states below or equivalent to 4^+ such as Ca^{2+}, $Mn^{2+,}$ Ni^{2+}, Cu^{2+}, Fe^{3+}, Co^{3+}, La^{3+}, and Y^{3+} (Palmqvist et al., 1998; Huang et al., 2012; Wu et al., 2015; Zedan and AlJaber, 2019). The presence of abundant oxygen vacancies promotes the mobility of lattice oxygen and subsequently boosts the catalytic activity of CeO_2. Meanwhile, there may also exist a synergistic effect between the doped metals and Ce. Palella *et al.* recently prepared $MnCeO_x$ composites *via* a redox route and demonstrated that Mn^{2+} ions are the active sites for the formation of active oxygen species arising from the oxygen vacancies in low-temperature oxidation of CH_4, while Ce elements can improve the availability of reactant molecules at the active site by introducing oxygen vacancies (Palella et al., 2021). There is a strong synergistic effect between Mn–Ce elements, which stabilizes Mn^{2+} species and facilitates the dispersion of Mn^{2+} ions. The dissociation of CH_4 into CH_n* and H* species was found to be the rate-determining step for the Mn-doped CeO_2 composite system. Apart from Mn, other monometallic elements such as Cu (T_{50} = 350°C), Fe (T_{50} = 378°C), Ni (T_{50} = 415°C), and Co (T_{50} = 380°C) catalysts have also improved catalytic activities and stabilities due to the established synergistic effects that increase the dispersion of active metal oxides, which allow more $M^{n+}/M^{(n-1)+}$ redox couples to participate in the redox cycle; more discussions on the doped CeO_2 catalysts can be found in a recent review by Stoian *et al.* in details (Stoian et al., 2021). Due to the absence of active site, which triggered by grain growth, CeO_2 is sintering at high temperature. Larrondo *et al.* tried to increase the thermal stability of CeO_2 by the addition of ZrO_2 to the structure of CeO_2 and found that ZrO_2 can also slightly facilitate the reducibility of the solids associated with both surface and bulk Ce sites with the evidence of H_2 TPR. And the catalysts with 10% of Zr have higher values of CH_4 conversion than the other

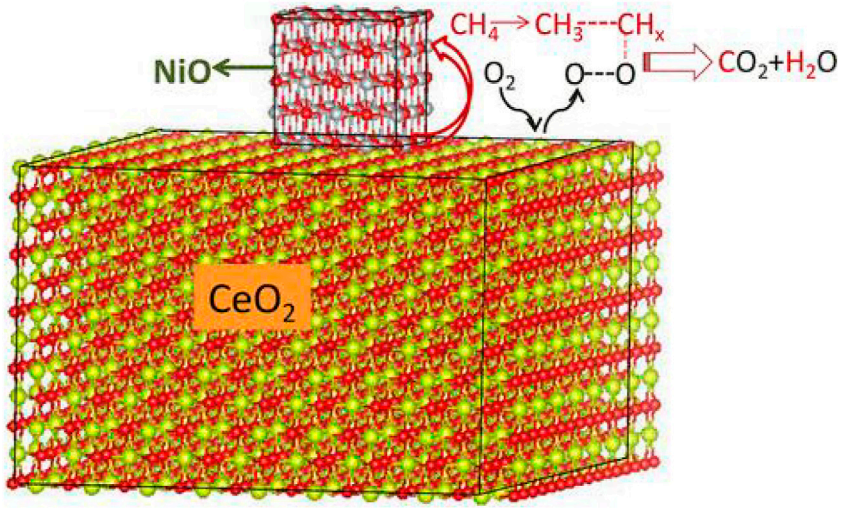

FIGURE 10
Schematic briefly showing activations of C–H of CH_4 and O–O of O_2 and coupling between CH_x species and atomic oxygen at the interface of NiO/CeO_2. Reprinted with permission from Zhang et al. (2018). Copyright (2018) American Chemical Society.

samples with 30% Zr and 50% Zr (Larrondo et al., 2005). Recently, Toscania *et al.* used the citrate complexation route to future prepared $Ce_{0.9}Sc_xZr_{0.1-x}O_{2-\delta}$ (x = 0, 0.02, 0.04, and 0.06) by citrate complexation route, with the aim of combining the improved thermal stability provided by the ZrO_2 with an increase in vacancy concentration upon Sc doping (Toscani et al., 2019). The doped samples exhibited superior redox behavior because the CeO_2 reduction values from TPR experiments and vacancy concentration from Raman tests both increase with increasing Sc content. And in contrast to the binary CeO_2–ZrO_2 sample, the CeO_2–ZrO_2–Sc_2O_3 showed the higher reaction rates and lower apparent activation energies for CMC. In addition, *in situ* XANES experiments confirm the participation of the lattice in the redox mechanism. Huang *et al.* prepared a series of NiO/CeO_2 by a facile impregnation method, which exhibited high catalytic performance and stability due to synergistic interaction between CeO_2 and NiO. The incorporation of Ni^{2+} into the CeO_2 lattice obviously enhanced the concentration of oxygen vacancies and amount of surface oxygen, making the mobility of bulk oxygen in CeO_2 increased, along with the reduction of the activation energy of the CMC. On the other hand, CeO_2 prevented the aggregation of NiO, further improving the reduction properties of NiO (Huang et al., 2020). Apart from this, CeO_2-modified catalytic materials can also be used in the reaction of oxidative coupling of methane (OCM) because of its above redox properties and increased surface basicity (Siakavelas et al., 2021). OCM is an exothermic reaction between CH_4 and O_2 in the range of 700–900°C, forming C_2 hydrocarbons (e.g., C_2H_4 or C_2H_6), *via* CH_4–CH_3–C_2H_6–C_2H_4 progress. Moreover, for OCM, the incorporation of *f*-block elements such as Pr^{3+}, Sm^{3+}, and La^{3+} (redox-active basic ions) into the CeO_2 could modify the acid–base properties, enhance its thermal stability, and generate additional oxygen vacancy sites (Xu et al., 2019; Zhang et al., 2020; Siakavelas et al., 2022a). Furthermore, Siakavelas et al. (2022b) recently added lithium ions into CeO_2- and CeO_2-modified materials (Sm-Ce and La-Sm-Ce metal oxides), using the wet impregnation technique. They argued that the addition of lithium species changed the reaction pathway and drastically enhanced the production of ethylene and ethane, mainly for the promoted catalysts (Li/Sm-Ce and Li/La-Sm-Ce).

3.6.3 Binary CeO_2 catalysts

The CMC involves both the activation of C–H of CH_4 and O–O of O_2. CeO_2 can activate molecular oxygen *via* Ce^{4+} and Ce^{3+} redox couples; however, it is incapable of activating the C–H of CH_4. On the contrary, NiO exhibits high activity in activating C–H, but, does not activate molecular oxygen. Thus, Zhang *et al.* synthesized NiO/CeO_2 through a two-step method, in which nanocomposite consists of CeO_2 nanorods with supported NiO nanoclusters, exhibiting notably higher activity due to the lowest apparent activation energy (69.4 ± 4 kJ/mol). The schematic diagram of the reaction mechanism at the interface is shown in Figure 10. The C–H of CH_4 was activated on the Ni-O species, forming a H_3C–Ni- intermediate on the interface. The formed CH_3 could be further activated to form CH_2 or even CH species, which could couple with surface lattice oxygen atoms to form CO_2 and H_2. The process follows the MvK mechanism, in which NiO nanoclusters and CeO_2 nanorods show a synergistic effect for CMC (Zhang et al., 2018).

3.6.4 Mechanisms

In conclusion, the mechanism of CeO_2 in CMC has been reported to follow the MvK mechanism (Knapp and Ziegler, 2008). Results reported in the literature indicate that the first step is hydrogen abstraction from the CH_4 molecule over the Ce surface. As the (111) surface of CeO_2 is the most stable and predominant, therefore, the exposed oxygen atoms with low coordination on the (111) surface are assumed as the active sites over CeO_2-based catalysts in CMC. CH_4 dissociation is followed by the formation of a CH_3 radical and an adsorbed H* atom. These two species bind to two surface oxygen atoms, leading to the formation of a methyl radical (CH_3^-) and a hydroxyl radical (HO·). Hydrogen adsorption leads to the reduction of one of the neighboring Ce atoms. Afterward, a series of intermediate steps take place, in which the H atoms are abstracted from CH_3* to form CH_2* and CH* until CO is formed by further reducing the Ce with the formation of an oxygen vacancy. Finally, the adsorbed CO reduces Ce by binding with another oxygen allowing the formation of CO_2. Water is formed by the binding of adjacent OH groups. The breaking of the C–H bond is generally the rate-limiting step in all methane activation processes (Tang et al., 2010).

3.7 CuO-based catalysts

3.7.1 Single CuO

CuO is an important p-type semiconducting material with a cubic rock salt structure (c-CuO) and lower-symmetry monoclinic structure (m-CuO). Analysis of the calculated band structures revealed that c-CuO is an indirect gap semiconductor, while m-CuO has metallic behavior (Cao et al., 2018). CuO has been considered as one of the most effective alternatives to noble metal-based catalysts in CMC because of its Earth abundance, non-toxicity, and good catalytic performance (Liu et al., 2010).

Researchers exhibited that Cu loading and the nature of the carrier exert influence on the Cu species present on the catalyst surface. Park and Ledford tested the catalytic activity of Cu/Al_2O_3 catalysts with different Cu loadings for CH_4 combustion reactions and they found that, with increasing Cu content, both the activity per unit mass of Cu and per mole of Cu on the surface decreased (Park and Ledford, 1998). The active phase for CH_4 oxidation is a superficial phase formed by isolated or highly dispersed Cu; as the Cu content increases, the dispersion becomes worse and therefore reduces the total number of active sites. Aguila *et al.* investigated CuO-loaded catalysts with porous media such as Al_2O_3, ZrO_2, and SiO_2 prepared by the impregnation method (Aguila et al., 2008). This work showed that CuO catalysts supported on ZrO_2 have higher activity (per unit mass of Cu) for CH_4 oxidation than when CuO is supported on alumina or silica, which is related to the ability of ZrO_2, stabilizing the highly dispersed Cu species to prevent the formation of bulk CuO. This ability is available when Cu concentrations between 0.25% and 6% for the catalysts are supported on ZrO_2. In addition, they also tested the influence of water for the CuO catalysts supported on ZrO_2. The addition of water produces a decrease of the CH_4 conversion, but, as soon as the water flow is stopped, the catalyst recovers its initial activity, which means that inhibition with water is reversible, at least for the 300 min considered in this experiment.

In addition to dispersion, the acid–base properties of the supports also affect the catalytic performance of Cu-based catalysts. Theoretically, the adsorption and activation of hydrocarbons on oxide-based catalysts and the desorption of reaction products are related not only to the strength and distribution of the Lewis acidic metal cation sites but also to the concentration of lattice oxygen anions as the Lewis base sites (Vedrine et al., 1996). Specifically, the interaction of CH_4 with acid–base pairs on the catalyst surface leads to the heterolytic breakage of the C–H bond and the formation of CH_3^- and H^+ species chemisorbed on the acid and base sites, respectively. Stronger acidic sites enhance the interaction with the carbon anion and therefore facilitate surface catalytic combustion (Choudhary and Rane, 1991). By co-precipitation and calcination methods, Popescu *et al.* synthesized the CuO nanoparticles supported on mixed oxides of Al_2O_3, MgO, and Mg(Al)O and investigated their catalytic properties in the total oxidation of CH_4 (Popescu et al., 2017). Because, on the one hand, CH_4 activation involving the heterolytic C–H bond breaking needs acid–base pairs, on the other hand, the total oxidation reaction is favored in the presence of acid sites of high strengths, which strongly adsorb carbanions, thus undergoing surface reaction with oxygen. The CuMgAl(1)O (Mg/Al atomic ratios is 1) showed the highest activity as it not only contained strong acid sites (ca.50%), which was similar with the CuAlO (strong acid species), but also had strong basic sites (ca. 30%).

3.7.2 Doped CuO

Lu *et al.* prepared CuO–CeO_2 hybrid nanoparticle and created substantial amounts of Cu–Ce–O interfaces by gas-phase evaporation-induced self-assembly. CuO–CeO_2 exhibited excellent catalytic performances with a low light-off temperature, high activity, selectivity, and operation stability. The two possible mechanisms of CMC over CuO and CuO–CeO_2 are shown in Figure 11. The authors conjectured that two routes follow the MvK mechanism. However, the Cu–Ce–O interfacial metal–support interaction promotes the redox cycle of interface, in which CH_4 binds to the surface of CuO, while O_2 is simultaneously adsorbed on the oxygen vacancy of CeO_2, then dissociating to a surface-bound methyl group and oxygen atoms, respectively; after the release of H_2O, an oxygen vacancy

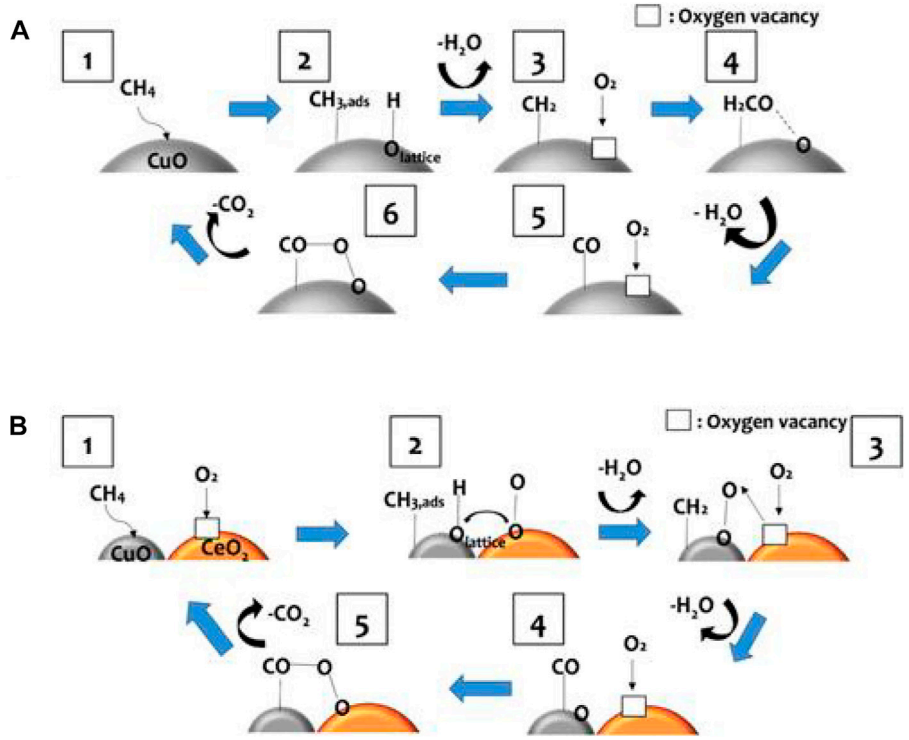

FIGURE 11
Cartoon depiction of methane combustion catalyzed by CuO **(A)** and Cu/CeO_2 **(B)**. Reprinted with permission from Lu et al. (2016). Copyright (2016) American Chemical Society.

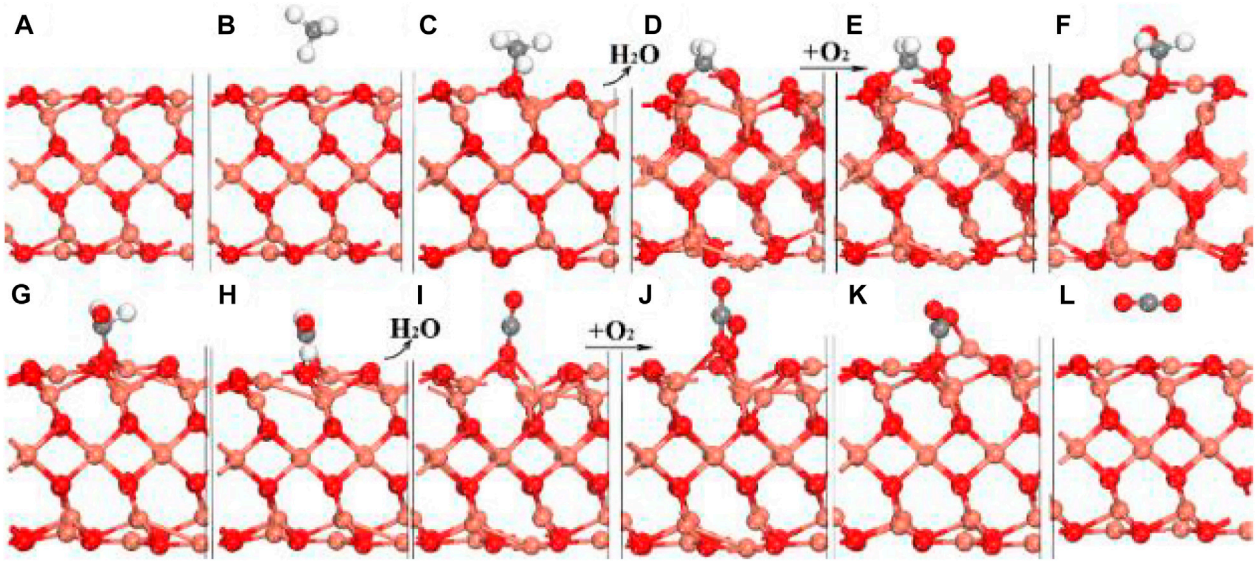

FIGURE 12
(A) Clean (001); **(B)** CH_4 physical adsorption; **(C)** CH_4 dissociative adsorption; **(D)** CH_2* with oxygen vacancy (OV) presented; **(E)** CH_2* with O_2 adsorbed; **(F)** CH_2* rotating and interacting with O_2*; **(G)** transition state (TS) state COH_2*; **(H)** CHO* + H*; **(I)** CO* with OV presented after releasing one H_2O; **(J)** CO* with O_2 adsorbed; **(K)** TS for O transfer to CO*; **(L)** CO_2 physical adsorbed. Cu, O, C, and H are shown as rose-carmine, red, grey and white spheres, respectively. Reprinted with permission from Kong et al. (2018). Copyright (2018) Beilstein-Institut.

regenerates, subsequently combining with the oxygen atoms; the dissociated methyl group is further oxidized by the adsorbed oxygen atoms, and then CO_2 is released from the surface of CuO. The synergistic effect between CuO and CeO_2 increases the rate of CMC, which has shown promise in enhancing the removal rate of hydrocarbon from the catalyst surface (Lu et al., 2016).

3.7.3 Mechanisms

Kong *et al.* identified CuO (001) as an active surface for CMC over CuO among other surfaces, including (110), (111), (101), (010), and (011) *via* DFT calculations (Figure 12). It is not surprising because (001) is strongly polarized and shows high reactivity due to the high ratio of lowly coordinated oxygen. In DFT calculations, CH_4 is firstly adsorbed with AE = -0.86 eV, followed by a spontaneous dissociation with CH_3 and H adsorbed on surface oxygen, as depicted in Figures 12A–C. Surface oxygen is often actively involved and may cleave H from CH_x to form -OH and H_2O, generating an oxygen vacancy (OV), which can be filled with reactant O_2, leading to its dissociation and further oxidizing CH_x intermediates, as shown in Figures 12D–F. With oxygen transferring to bond with carbon, the hydrogen in CH_x can shift to surface oxygen again with an energy release of 3.66 and 1.46 eV, indicating that such a shift is highly favorable, as shown in Figures 12G–I. Again, an OV is generated and refilled by O_2 when H_2O is released, and similarly O_2 is dissociated to release atomic oxygen after exceeding a small barrier of 0.47 eV, which can oxidize adsorbed CO to form CO_2, as outlined in Figures 12I–L. Although the authors did not specify which mechanism the mechanism of CMC over CuO (001) conforms to, given their theoretical calculations, we believe that it is consistent with the MvK mechanism (Kong et al., 2018).

4 Perspectives

It has been well acknowledged that TMOs are one of the most promising candidates as alternatives to noble metal catalysts in CMC. Although promises have seen in some TMOs, problems still exist such as the controversial reaction mechanism, low water vapor, and sulfur resistance. Therefore, it is necessary to explore appropriate preparation methods, suitable modified ions, and the optimal ratios to synthesize novel TMOs with excellent resistance to water vapor and sulfur poisoning, guided by the reaction mechanism (Lin et al., 2017; Chen et al., 2022).

Some TMOs with significant water resistance, such as NiO, should be further studied to enhance sulfur resistance. Cr_2O_3 with excellent sulfur resistance can be selected to prepare binary complexes to enhance its catalytic stability (Ordóñez et al., 2008). Although α-Fe_2O_3 catalysts, especially with two-dimensional nanostructure, have been proven to have excellent catalytic performance in CMC, their performance is significantly reduced in the presence of steam and SO_2. Herein, we can further investigate Fe–Cr mixed catalysts with the emphasis on the creation of spinel structures to increase the sulfur and water resistance of iron-based catalysts (García-Vázquez et al., 2020).

In addition, beyond complete oxidation, TMOs also find great uses in CH_4 partial oxidation reactions, such as direct oxidation to methanol, which is known as the "holy grail" in catalysis community to convert CH_4 into value-added chemicals with a much reduced cost in reaction steps and separation as compared to the conventional industrial route. (Sushkevich et al., 2017). The TMOs reveal the enormous potentials in the direct oxidation of CH_4 to CH_3OH owing to the relatively strong ability to activate the C–H bond and avoid CH_4 overoxidation.

In nature, CH_4 monooxygenase can directly convert CH_4 to CH_3OH using H_2O, O_2, and CO_2 as reactants at an ambient temperature (Sun et al., 2021). However, such biomimetic strategies are often limited by industrial-scale reactions. Some TMOs can dissociate CH_4 at room temperature, which offers the possibility for the direct conversion of CH_4 (Huang et al., 2021). Zuo *et al.* found that an inverse $CeO_2/Cu_2O/Cu$ (111) catalyst is able to bind and dissociate CH_4 at room temperature by mimicking the function of the CH_4 monooxygenase. The catalytic system produced only adsorbed CH_x fragments in the presence of H_2O, along with a high transformation from CH_4 to CH_3OH. The dissociation of H_2O formed OH groups, which occupied the catalyst surface. OH groups removed sites decomposing CH_x fragments, generating centers with special electronic properties. On the special active centers, CH_4 could directly interact to yield CH_3OH (Zuo et al., 2016). Liu *et al.* carefully studied key roles of H_2O for the conversion of CH_4 directly into CH_3OH on $CeO_2/Cu_2O/Cu$ (111). H_2O preferentially dissociated over the active Ce sites at the $CeO_2/Cu_2O/Cu$ (111) interface, hindering O_2 activation and the overoxidation of CH_4. H_2O produced active *OH to promote the direct conversion of CH_4. O_2 dominantly reoxidized the reduced CeO_x, and water adsorption also displaced the produced methanol into the gas phase (Liu et al., 2020).

Some researchers have explored bimetallic oxides with dual roles, in which one oxide activates CH_4 and the other ensures high selectivity to methanol. Yang *et al.* synthesized highly mixed hybrid IrO_2/CuO *via* a bottom-up tactic, which exhibited excellent catalytic performance with a methanol yield of 1937 μmol $gcat^{-1}$ and a methanol selectivity of about 95% through the synergistic effect of IrO_2 for CH_4 activation and CuO for selective oxidation. In the oxidation process of methane, due to the strong electrophilic property of Ir^{4+}, IrO_2 could facilitate the C–H bond cleavage by forming Ir-C σ bond. Then, -CH_3 attached by Ir bound to the neighboring Cu-attached O to form -OCH_3, subsequently extracted by H_2O to accelerate the formation of methanol.

At last, the formed O vacancy is replenished by O_2 (Yang et al., 2019).

It deserves to explore novel metal oxides with low metal-O bond strength and satisfactory methanol selectivity for facilitating the surface methoxy group formation. The metal oxides can also be employed as a cocatalyst being strong electrophilic metal oxides with extraordinary capacity to promote the C–H bond cleavage of CH_4 (Fuller et al., 2016). The synergistic effect of bimetallic oxides offers an alternative route for the design and synthesis of novel catalysts for the direct conversion of CH_4 into methanol (Lyu et al., 2021). In addition, the mechanism by which H_2O promotes the high selectivity of direct CH_4 conversion also needs to be continuously explored.

5 Conclusion

As an important greenhouse gas, the lean emission of CH_4 causes a huge environmental crisis. In this article, all the described results certify that both single and binary TMOs show the great potential of being promising alternatives to the expensive noble metal catalysts. Reviewed novel TMO catalysts exhibit appreciable catalytic reactivity associated with preparation methods, structures, morphologies, exposed crystal planes, crystal defects, oxygen vacancies, doping, and supporting. It can be seen that the structure, morphology, and exposed crystal planes determined by the preparation method significantly influence their catalytic activity for the CMC through the variation in morphology, surface area, and surface or lattice defects. In addition, mixed TMO catalysts prepared by doping and supporting exhibit excellent catalytic performance compared with the corresponding single TMOs due to synergistic interactions between the different TMO species. In general, the deactivation of TMO catalysts due to water vapor poisoning is reversible, while the deactivation due to sulfur poisoning is irreversible. The doping and supporting will improve the stability of TMO catalysts. The reaction mechanism of CMC over TMO catalysts is still controversial. Among the discussed possibilities, the MvK mechanism involves the oxidation of methane only by lattice oxygen with molecular oxygen replenishing the lattice oxygen after its consumption, while the L–H and E–R mechanisms only involve surface-adsorbed oxygen from molecular oxygen in the gas phase as the oxidizing power for methane activation. In addition, the T-T mechanism is also proposed for reactions involving both surface-adsorbed oxygen and lattice oxygen. The dominance of surface-adsorbed oxygen and lattice oxygen may change with the catalyst structure and temperature. As the characteristic techniques are under progressive development, it is expected to reveal the precise reaction mechanism of CMC over different TMO catalytic systems and therefore the identification of the true active site structures.

Author contributions

YG and MJ drafted the article, conceived the concept of the review, conducted literature survey, and arranged the figures. LY, ZL, FT, and YH revised the article and provided comments. All authors contributed to the article and approved the submitted version.

Funding

This project was financially supported by the Shanghai Post-Doctoral Excellence Program, 2021232, and the UM-SJTU Joint Institute and Shanghai Science and Technology Development Funds of “Rising Star” Sailing Program (22YF1419400).

Conflict of interest

The authors declare that the research was conducted in the absence of any commercial or financial relationships that could be construed as a potential conflict of interest.

Publisher’s note

All claims expressed in this article are solely those of the authors and do not necessarily represent those of their affiliated organizations, or those of the publisher, the editors, and the reviewers. Any product that may be evaluated in this article, or claim that may be made by its manufacturer, is not guaranteed or endorsed by the publisher.

References

Aguila, G., Gracia, F., Cortés, J., and Araya, P. (2008). Effect of copper species and the presence of reaction products on the activity of methane oxidation on supported CuO catalysts. *Appl. Catal. B Environ.* 77 (3-4), 325–338. doi:10.1016/j.apcatb.2007.08.002

Akbari, E., Alavi, S. M., Rezaei, M., and Larimi, A. (2021). Catalytic methane combustion on the hydrothermally synthesized MnO_2 nanowire catalysts. *Ind. Eng. Chem. Res.* 60, 7572–7587. doi:10.1021/acs.iecr.1c00881

Aneggi, E., Boaro, M., Colussi, S., de Leitenburg, C., and Trovarelli, A. (2016). Ceria-based materials in catalysis: Historical perspective and future trends. *Handb. Phys. Chem. Rare Earths* 50, 209–242. doi:10.1016/bs.hpcre.2016.05.002

Arena, F., Di Chio, R., Fazio, B., Espro, C., Spiccia, L., Palella, A., et al. (2017). Probing the functionality of nanostructured $MnCeO_x$ catalysts in the carbon monoxide oxidation. *Appl. Catal. B Environ.* 210, 14–22. doi:10.1016/j.apcatb.2017.03.049

Barbosa, A. L., Herguido, J., and Santamaria, J. (2001). Methane combustion over unsupported iron oxide catalysts. *Catal. Today* 64 (1-2), 43–50. doi:10.1016/S0920-5861(00)00507-1

Becker, E., Carlsson, P. A., Kylhammar, L., Newton, M. A., and Skoglundh, M. (2011). *In situ* spectroscopic investigation of low-temperature oxidation of methane over alumina-supported platinum during periodic operation. *J. Phys. Chem. C* 115, 944–951. doi:10.1021/jp103609n

Belessi, V. C., Ladavos, A. K., Armatas, G. S., and Pomonis, P. J. (2001). Kinetics of methane oxidation over La-Sr-Ce-Fe-O mixed oxide solids. *Phys. Chem. Chem. Phys.* 3 (17), 3856–3862. doi:10.1039/b103426j

Buchneva, O., Gallo, A., and Rossetti, I. (2012). Effect of nitrogen-containing impurities on the activity of perovskitic catalysts for the catalytic combustion of methane. *Inorg. Chem.* 51 (21), 11680–11687. doi:10.1021/ic3015892

Cao, H., Zhou, Z., Yu, J., and Zhou, X. (2018). DFT study on structural, electronic, and optical properties of cubic and monoclinic CuO. *J. Comput. Electron.* 17 (1), 21–28. doi:10.1007/s10825-017-1057-9

Chen, J. H., Arandiyan, H., Gao, X., and Li, J. H. (2015). Recent advances in catalysts for methane combustion. *Catal. Surv. Asia* 19 (3), 140–171. doi:10.1007/s10563-015-9191-5

Chen, K., Li, W. Z., Li, X. Z., Ogunbiyi, A. T., and Yuan, L. (2021). Irregularly shaped NiO nanostructures for catalytic lean methane combustion. *ACS Appl. Nano Mat.* 4 (5), 5404–5412. doi:10.1021/acsanm.1c00732

Chen, Y. L., Lin, J., Chen, X. H., Fan, S. Q., and Zheng, Y. (2021). Engineering multicomponent metal-oxide units for efficient methane combustion over palladium-based catalysts. *Catal. Sci. Technol.* 11 (1), 152–161. doi:10.1039/d0cy01742f

Chen, Y., Yao, K., Zhang, X., Shen, B., Smith, R. L., Jr, Guo, H., et al. (2022). Siloxane-modified MnO_x catalyst for oxidation of coal-related o-xylene in presence of water vapor. *J. Hazard. Mat.* 436, 129109. doi:10.1016/j.jhazmat.2022.129109

Chen, Z. P., Wang, S., Liu, W. G., Gao, X. H., Gao, D. N., Wang, M. Z., et al. (2016). Morphology-dependent performance of Co_3O_4 *via* facile and controllable synthesis for methane combustion. *Appl. Catal. A General* 525, 94–102. doi:10.1016/j.apcata.2016.07.009

Cheng, Z., Qin, L., Guo, M., Xu, M., Fan, J. A., Fan, L. S., et al. (2016). Oxygen vacancy promoted methane partial oxidation over iron oxide oxygen carriers in the chemical looping process. *Phys. Chem. Chem. Phys.* 18 (47), 32418–32428. doi:10.1039/C6CP06264D

Choudhary, V., and Rane, V. H. (1991). Acidity/basicity of rare-earth oxides and their catalytic activity in oxidative coupling of methane to C_2-hydrocarbons. *J. Catal.* 130 (2), 411–422. doi:10.1016/0021-9517(91)90124-M

Choya, A., de Rivas, B., González-Velasco, J. R., Gutiérrez-Ortiz, J. I., and López-Fonseca, R. (2018a). Oxidation of residual methane from VNG vehicles over Co_3O_4-based catalysts: Comparison among bulk, Al_2O_3-supported and Ce-doped catalysts. *Appl. Catal. B Environ.* 237, 844–854. doi:10.1016/j.apcatb.2018.06.050

Choya, A., de Rivas, B., Gutiérrez-Ortiz, J. I., and López-Fonseca, R. (2018b). Effect of residual Na^+ on the combustion of methane over Co_3O_4 bulk catalysts prepared by precipitation. *Catalysts* 8 (10), 427. doi:10.3390/catal8100427

Choya, A., Gudyka, S., de Rivas, B., Gutiérrez-Ortiz, J. I., Kotarba, A., López-Fonseca, R., et al. (2021). Design, characterization and evaluation of Ce-modified cobalt catalysts supported on alpha alumina in the abatement of methane emissions from natural gas engines. *Appl. Catal. A General* 617, 118105. doi:10.1016/j.apcata.2021.118105

Choya, A., Rivas, B. D., Gutiérrez-Ortiz, J. I., and López-Fonseca, R. (2022). Bulk Co_3O_4 for methane oxidation: Effect of the synthesis route on physico-chemical properties and catalytic performance. *Catalysts* 12, 87. doi:10.3390/catal12010087

Cornell, R. M., and Schwertmann, U. (2003). *The iron oxides: Structure, properties, reactions, occurrences, and uses*, 2. Weinheim: Wiley VCH, 71. doi:10.1515/CORRREV.1997.15.3-4.533

Dong, B., Zhang, H., Kong, A., Kong, Y., Yang, F., Shan, Y., et al. (2014). Synthesis of urchin-Like FeF_2 nanoarchitectures and their conversion into three-dimensional urchin-like mesoporous α-Fe_2O_3 nanoarchitectures for methane activation. *Eur. J. Inorg. Chem.* 28, 4779–4787. doi:10.1002/ejic.201402152

Dou, J., Tang, Y., Nie, L., Andolina, C. M., Zhang, X., House, S., et al. (2018). Complete oxidation of methane on Co_3O_4/CeO_2 nanocomposite: A synergic effect. *Catal. Today* 311, 48–55. doi:10.1016/j.cattod.2017.12.027

Dupont, N., Kaddouri, A., and Gélin, P. (2010). Physicochemical and catalytic properties of sol gel-prepared copper-chromium oxides. *J. Solgel. Sci. Technol.* 58 (1), 302–306. doi:10.1007/s10971-010-2391-6

El-Sheikh, S. M., Mohamed, R. M., and Fouad, O. A. (2009). Synthesis and structure screening of nanostructured chromium oxide powders. *J. Alloys Compd.* 482 (1-2), 302–307. doi:10.1016/j.jallcom.2009.04.011

Fan, S. Q., Zhang, W., Xu, H., Cai, G. H., Zhan, Y. Y., Chen, X. H., et al. (2022). Tuning lattice defects to facilitate the catalytic performance of Ni-Cu-O hybrid nanoparticles towards methane oxidation. *Int. J. Hydrogen Energy* 47, 4536–4545. doi:10.1016/j.ijhydene.2021.11.060

Feng, Z. J., Du, C., Chen, Y. J., Lang, Y., Zhao, Y. K., Cho, K., et al. (2018). Improved durability of Co_3O_4 particles supported on $SmMn_2O_5$ for methane combustion. *Catal. Sci. Technol.* 8 (15), 3785–3794. doi:10.1039/c8cy00897c

Feyel, S., Döbler, J., Schröder, D., Sauer, J., and Schwarz, H. (2006). Thermal activation of methane by tetranuclear $[V_4O_{10}]^+$. *Angew. Chem. Int. Ed.* 45 (28), 4681–4685. doi:10.1002/anie.200600188

Fu, G., Xu, X., and Wan, H. L. (2006). Mechanism of methane oxidation by transition metal oxides: A cluster model study. *Catal. Today* 117 (1-3), 133–137. doi:10.1016/j.cattod.2006.05.048

Fuller, J. T., Butler, S., Devarajan, D., Jacobs, A., Hashiguchi, B. G., Konnick, M. M., et al. (2016). Catalytic mechanism and efficiency of methane oxidation by Hg (II) in sulfuric acid and comparison to radical initiated conditions. *ACS Catal.* 6 (7), 4312–4322. doi:10.1021/acscatal.6b00226

García-Vázquez, M., Wang, K., González-Carballo, J. M., Brown, D., Landon, P., Tooze, R., et al. (2020). Iron and chromium-based oxides for residual methane abatement under realistic conditions: A study on sulfur dioxide poisoning and steam-induced inhibition. *Appl. Catal. B Environ.* 277, 119139. doi:10.1016/j.apcatb.2020.119139

Gong, D., and Zeng, G. F. (2021). Low-temperature combustion of methane over graphene templated Co_3O_4 defective-nanoplates. *Sci. Rep.* 11, 12604. doi:10.1038/s41598-021-92165-4

Gremminger, A., Lott, P., Merts, M., Casapu, M., Grunwaldt, J. D., Deutschmann, O., et al. (2017). Sulfur poisoning and regeneration of bimetallic Pd-Pt methane oxidation catalysts. *Appl. Catal. B Environ.* 218, 833–843. doi:10.1016/j.apcatb.2017.06.048

Han, Y. F., Chen, L. W., Ramesh, K., Widjaja, E., Chilukoti, S., Surjami, I. K., et al. (2008). Kinetic and spectroscopic study of methane combustion over α-Mn_2O_3 nanocrystal catalysts. *J. Catal.* 253 (2), 261–268. doi:10.1016/j.jcat.2007.11.010

Han, Z., Zhang, H. Q., Dong, B., Ni, Y. Y., Kong, A. G., Shan, Y. K., et al. (2016). High efficient mesoporous Co_3O_4 nanocatalysts for methane combustion at low temperature. *ChemistrySelect* 5, 979–983. doi:10.1002/slct.201600211

He, L., Fan, Y. L., Bellettre, J., Yue, J., and Luo, L. G. (2020). A review on catalytic methane combustion at low temperatures: Catalysts, mechanisms, reaction conditions and reactor designs. *Renew. Sustain. Energy Rev.* 119, 109589. doi:10.1016/j.rser.2019.109589

He, Y. L., Y. L., Guo, F. C., Yang, K. R., Heinlein, J. A., Bamonte, S. M., Fee, J. J., et al. (2020). *In situ* identification of reaction intermediates and mechanistic understandings of methane oxidation over hematite: A combined experimental and theoretical study. *J. Am. Chem. Soc.* 142 (40), 17119–17130. doi:10.1021/jacs.0c07179

Horn, R., and Schlögl, R. (2014). Methane activation by heterogeneous catalysis. *Catal. Lett.* 145 (1), 23–39. doi:10.1007/s10562-014-1417-z

Hu, L. H., Peng, Q., and Li, Y. D. (2008). Selective synthesis of Co_3O_4 nanocrystal with different shape and crystal plane effect on catalytic property for methane combustion. *J. Am. Chem. Soc.* 130 (48), 16136–16137. doi:10.1021/ja806400e

Hu, W. D., Lan, J. G., Guo, Y., Cao, X. M., and Hu, P. (2016). Origin of efficient catalytic combustion of methane over Co_3O_4(110): Active low-coordination lattice oxygen and cooperation of multiple active sites. *ACS Catal.* 6 (8), 5508–5519. doi:10.1021/acscatal.6b01080

Huang, E., Orozco, I., Ramírez, P. J., Liu, Z. Y., Zhang, F., Mahapatra, M., et al. (2021). Selective methane oxidation to methanol on ZnO/Cu_2O/Cu (111) catalysts: Multiple site-dependent behaviors. *J. Am. Chem. Soc.* 143, 19018–19032. doi:10.1021/jacs.1c08063

Huang, L., Zhang, X., Lin, C. H. E. N., and Lecheng, L. (2012). Promotional effect of CeO_2 and Y_2O_3 on CuO/ZrO_2 catalysts for methane combustion. *J. Rare Earths* 30 (2), 123–127. doi:10.1016/S1002-0721(12)60007-6

Huang, W., Zha, W. W., Zhao, D. L., and Feng, S. J. (2019). The effect of active oxygen species in nano-$ZnCr_2O_4$ spinel oxides for methane catalytic combustion. *Solid State Sci.* 87, 49–52. doi:10.1016/j.solidstatesciences.2018.11.006

Huang, X., Li, J., Wang, J., Li, Z., and Xu, J. (2020). Catalytic combustion of methane over a highly active and stable NiO/CeO_2 catalyst. *Front. Chem. Sci. Eng.* 14 (4), 534–545. doi:10.1007/s11705-019-1821-4

Jia, J. B., Ran, R., Guo, R. Q., Wu, X. D., and Weng, D. (2018). ZrO_2-supported α-MnO_2: Improving low-temperature activity and stability for catalytic oxidation of methane. *Prog. Nat. Sci. Mater. Int.* 28, 296–300. doi:10.1016/j.pnsc.2018.04.005

Jia, J. B., Ran, R., Wu, X. D., Chen, W., Si, Z. C., Weng, D., et al. (2019). Tuning nonstoichiometric defects in single-phase MnO_x for methane complete oxidation. *Mol. Catal.* 467, 120–127. doi:10.1016/j.mcat.2019.01.032

Jia, J. B., Zhang, P. Y., and Chen, L. (2016). Catalytic decomposition of gaseous ozone over manganese dioxides with different crystal structures. *Appl. Catal. B Environ.* 189, 210–218. doi:10.1016/j.apcatb.2016.02.055

Jia, Y. C., Wang, S. Y., Lu, J. Q., and Luo, M. F. (2016). Effect of structural properties of mesoporous Co_3O_4 catalysts on methane combustion. *Chem. Res. Chin. Univ.* 32 (5), 808–811. doi:10.1007/s40242-016-6141-3

Jodłowski, P. J., Chlebda, D., Piwowarczyk, E., Chrzan, M., Jędrzejczyk, R. J., Sitarz, M., et al. (2016). *In situ* and operando spectroscopic studies of sonically aided catalysts for biogas exhaust abatement. *J. Mol. Struct.* 1126, 132–140. doi:10.1016/j.molstruc.2016.02.039

Kašpar, J., Fornasiero, P., and Graziani, M. (1999). Use of CeO_2-based oxides in the three-way catalysis. *Catal. Today* 50 (2), 285–298. doi:10.1016/S0920-5861(98)00510-0

Knapp, D., and Ziegler, T. (2008). Methane dissociation on the ceria (111) surface. *J. Phys. Chem. C* 112 (44), 17311–17318. doi:10.1021/jp8039862

Kong, Q., Yin, Y., Xue, B., Jin, Y., Feng, W., Chen, Z. G., et al. (2018). Improved catalytic combustion of methane using CuO nanobelts with predominantly (001) surfaces. *Beilstein J. Nanotechnol.* 9 (1), 2526–2532. doi:10.3762/bjnano.9.235

Kuo, C. H., Li, W. K., Song, W. Q., Luo, Z., Poyraz, A. S., Guo, Y., et al. (2014). Facile synthesis of Co_3O_4@CNT with high catalytic activity for CO oxidation under moisture-rich conditions. *ACS Appl. Mat. Interfaces* 6, 11311–11317. doi:10.1021/am501815d

Larrondo, S., Vidal, M. A., Irigoyen, B., Craievich, A. F., Lamas, D. G., and Fábregas, I. O. (2005). Preparation and characterization of Ce/Zr mixed oxides and their use as catalysts for the direct oxidation of dry CH_4. *Catal. Today* 53–59. doi:10.1016/j.cattod.2005.07.110

Li, J. A., Li, M. M., Gui, P., Zheng, L. N., Liang, J. S., Xue, G., et al. (2019). Hydrothermal synthesis of sandwich interspersed $LaCO_3OH/Co_3O_4$/graphene oxide composite and the enhanced catalytic performance for methane combustion. *Catal. Today* 327, 134–142. doi:10.1016/j.cattod.2018.05.027

Li, J. H., Liang, X., Xu, S. C., and Hao, J. M. (2009). Catalytic performance of manganese cobalt oxides on methane combustion at low temperature. *Appl. Catal. B Environ.* 90 (1-2), 307–312. doi:10.1016/j.apcatb.2009.03.027

Li, J. L., Zhou, S. D., Zhang, J., Schlangen, M., Usharani, D., Shaik, S., et al. (2016). Mechanistic variants in gas-phase metal-oxide mediated activation of methane at ambient conditions. *J. Am. Chem. Soc.* 138 (35), 11368–11377. doi:10.1021/jacs.6b07246

Li, K., Liu, K., Xu, D. J., Ni, H., Shen, F. X., Chen, T., et al. (2019). Lean methane oxidation over $Co_3O_4/Ce_{0.75}Zr_{0.25}$ catalysts at low-temperature: Synergetic effect of catalysis and electric field. *Chem. Eng. J.* 369, 660–671. doi:10.1016/j.cej.2019.03.059

Li, L., Chen, H. W., Zhang, C. Y., and Fei, Z. Y. (2019). Ultrafine cobalt oxide nanoparticles embedded in porous SiO_2 matrix as efficient and stable catalysts for methane combustion. *Mol. Catal.* 469, 155–160. doi:10.1016/j.mcat.2018.12.028

Li, M. M., Gui, P., Zheng, L. N., Li, J. A., Xue, G., Liang, J. S., et al. (2018). Active component migration and catalytic properties of nitrogen modified composite catalytic materials. *Catalysts* 8 (4), 125. doi:10.3390/catal8040125

Li, Y. X., Guo, Y. H., and Xue, B. (2009). Catalytic combustion of methane over M (Ni, Co, Cu) supported on ceria-magnesia. *Fuel Process. Technol.* 90 (5), 652–656. doi:10.1016/j.fuproc.2008.12.002

Liang, Z., Li, T., Kim, M., Asthagiri, A., and Weaver, J. F. (2017). Low-temperature activation of methane on the IrO_2(110) surface. *Science* 356, 299–303. doi:10.1126/science.aam9147

Lin, F. W., Wang, Z. H., Shao, J. M., Yuan, D. K., He, Y., Zhu, Y. Q., et al. (2017). Catalyst tolerance to SO_2 and water vapor of Mn based bimetallic oxides for NO deep oxidation by ozone. *RSC Adv.* 7 (40), 25132–25143. doi:10.1039/c7ra04010e

Liu, C., Xian, H., Jiang, Z., Wang, L. H., Zhang, J., Zheng, L. R., et al. (2015). Insight into the improvement effect of the Ce doping into the SnO_2 catalyst for the catalytic combustion of methane. *Appl. Catal. B Environ.* 176-177, 542–552. doi:10.1016/j.apcatb.2015.04.042

Liu, F. X., Sang, Y. Y., Ma, H. W., Li, Z. P., and Gao, Z. M. (2017). Nickel oxide as an effective catalyst for catalytic combustion of methane. *J. Nat. Gas. Sci. Eng.* 41, 1–6. doi:10.1016/j.jngse.2017.02.025

Liu, L., Yao, Z., Liu, B., and Dong, L. (2010). Correlation of structural characteristics with catalytic performance of $CuO/Ce_xZr_{1-x}O_2$ catalysts for NO reduction by CO. *J. Catal.* 275 (1), 45–60. doi:10.1016/j.jcat.2010.07.024

Liu, Z., Huang, E., Orozco, I., Liao, W. J., Palomino, R. M., Rui, N., et al. (2020). Water-promoted interfacial pathways in methane oxidation to methanol on a CeO_2-Cu_2O catalyst. *Science* 368, 513–517. doi:10.1126/science.aba5005

Lu, Y. F., Chou, F. C., Lee, F. C., Lin, C. Y., and Tsai, D. H. (2016). Synergistic catalysis of methane combustion using Cu-Ce-O hybrid nanoparticles with high activity and operation stability. *J. Phys. Chem. C* 120 (48), 27389–27398. doi:10.1021/acs.jpcc.6b09441

Lyu, Y. M., Jocz, J. N., Xu, R., Williams, O. C., and Sievers, C. (2021). Selective oxidation of methane to methanol over ceria-zirconia supported mono and bimetallic transition metal oxide catalysts. *ChemCatChem* 13 (12), 2832–2842. doi:10.1002/cctc.202100268

Mukherjee, D., Rao, B. G., and Reddy, B. M. (2016). CO and soot oxidation activity of doped ceria: Influence of dopants. *Appl. Catal. B Environ.* 197, 105–115. doi:10.1016/j.apcatb.2016.03.042

Neatu, S., Trandafir, M. M., Stănoiu, A., Florea, O. G., Simion, C. E., Leonat, L. N., et al. (2019). Bulk versus surface modification of alumina with Mn and Ce based oxides for CH_4 catalytic combustion. *Materials* 12 (11), 1771. doi:10.3390/ma12111771

Ordóñez, S., Paredes, J. R., and Díez, F. V. (2008). Sulphur poisoning of transition metal oxides used as catalysts for methane combustion. *Appl. Catal. A General* 341 (1-2), 174–180. doi:10.1016/j.apcata.2008.02.042

Palella, A., Spadaro, L., Di Chio, R., and Arena, F. (2021). Effective low-temperature catalytic methane oxidation over $MnCeO_x$ catalytic compositions. *Catal. Today* 379, 240–249. doi:10.1016/j.cattod.2020.11.010

Palmqvist, A. E. C., Johansson, E. M., Järås, S. G., and Muhammed, M. (1998). Total oxidation of methane over doped nanophase cerium oxides. *Catal. Lett.* 56 (1), 69–75. doi:10.1023/A:1019032306894

Paredes, J. R., Dı´az, E., Dı´ez, F. V., and Ordo´ñez, S. (2009). Combustion of methane in lean mixtures over bulk transition-metal oxides: Evaluation of the activity and self-deactivation. *Energy fuels.* 23 (1), 86–93. doi:10.1021/ef800704e

Paredes, J. R., Ordóñez, S., Vega, A., and Dıez, F. V. (2004). Catalytic combustion of methane over red mud-based catalysts. *Appl. Catal. B Environ.* 47 (1), 37–45. doi:10.1016/S0926-3373(03)00325-4

Park, P. W., and Ledford, J. S. (1998). The influence of surface structure on the catalytic activity of alumina supported copper oxide catalysts. Oxidation of carbon monoxide and methane. *Appl. Catal. B Environ.* 15 (3-4), 221–231. doi:10.1016/S0926-3373(98)80008-8

Pecchi, G., Jiliberto, M. G., Buljan, A., and Delgado, E. J. (2011). Relation between defects and catalytic activity of calcium doped $LaFeO_3$ perovskite. *Solid State Ionics* 187 (1), 27–32. doi:10.1016/j.ssi.2011.02.014

Pecchi, G., Reyes, P., Zamora, R., López, T., and Gómez, R. (2005). Effect of the promoter and support on the catalytic activity of Pd-CeO_2-supported catalysts for CH_4 combustion. *J. Chem. Technol. Biotechnol.* 80 (3), 268–272. doi:10.1002/jctb.1120

Pfefferle, L. D., and Pfefferle, W. C. (1987). Catalysis in combustion. *Catal. Rev.* 29 (2-3), 219–267. doi:10.1080/01614948708078071

Popescu, I., Tanchoux, N., Tichit, D., and Marcu, I. C. (2017). Total oxidation of methane over supported CuO: Influence of the Mg_xAl_yO support. *Appl. Catal. A General* 538, 81–90. doi:10.1016/j.apcata.2017.03.012

Pratt, C., and Tate, K. (2018). Mitigating methane: Emerging technologies to combat climate change's second leading contributor. *Environ. Sci. Technol.* 52, 6084–6097. doi:10.1021/acs.est.7b04711

Pu, Z. Y., Liu, Y., Zhou, H., Huang, W. Z., Zheng, Y. F., Li, X. N., et al. (2017). Catalytic combustion of lean methane at low temperature over ZrO_2-modified Co_3O_4 catalysts. *Appl. Surf. Sci.* 422, 85–93. doi:10.1016/j.apsusc.2017.05.231

Raj, B. A. (2016). Methane emission control. *Johns. Matthey Technol. Rev.* 60 (4), 228–235. doi:10.1595/205651316X692554

Rodríguez-Fernández, J., Sun, Z. Z., Zhang, L., Tan, T., Curto, A., Fester, J., et al. (2019). Structural and electronic properties of Fe dopants in cobalt oxide nanoislands on Au(111). *J. Chem. Phys.* 150, 041731. doi:10.1063/1.5052336

Ross, M. O., and Rosenzweig, A. C. (2017). A tale of two methane monooxygenases. *J. Biol. Inorg. Chem.* 22, 307–319. doi:10.1007/s00775-016-1419-y

Sanchis, R., García, A., Ivars-Barceló, F., Taylor, S. H., García, T., Dejoz, A., et al. (2021). Highly active Co_3O_4-based catalysts for total oxidation of light C_1-C_3 alkanes prepared by a simple soft chemistry method: Effect of the heat-treatment temperature and mixture of alkanes. *Materials* 14, 7120. doi:10.3390/ma14237120

Seeburg, D., Liu, D. J., Radnik, J., Atia, H., Pohl, M. M., Schneider, M., et al. (2018). Structural changes of highly active Pd/MeO_x (Me = Fe, Co, Ni) during catalytic methane combustion. *Catalysts* 8 (2), 42. doi:10.3390/catal8020042

Setiawan, A., Kennedy, E. M., Dlugogorski, B. Z., Adesina, A. A., and Stockenhuber, M. (2015). The stability of Co_3O_4, Fe_2O_3, Au/Co_3O_4 and Au/Fe_2O_3 catalysts in the catalytic combustion of lean methane mixtures in the presence of water. *Catal. Today* 258, 276–283. doi:10.1016/j.cattod.2014.11.031

Shu, Y., Wang, M. Y., Duan, X. L., Liu, D. D., Yang, S. Z., Zhang, P. F., et al. (2022). Low-temperature total oxidation of methane by pore- and vacancy-engineered NiO catalysts. *AIChE J.* 68 (6), e17664. doi:10.1002/aic.17664

Siakavelas, G. I., Charisiou, N. D., AlKhoori, A., Gaber, S., Sebastian, V., and Hinder, S. J. (2022b). Oxidative coupling of methane on Li/CeO_2 based catalysts: Investigation of the effect of Mg- and La-doping of the CeO_2 support. *Mol. Catal.* 520, 112157. doi:10.1016/j.mcat.2022.112157

Siakavelas, G. I., Charisiou, N. D., AlKhoori, A., Sebastian, V., Hinder, S. J., and Baker, M. (2022a). Cerium oxide catalysts for oxidative coupling of methane reaction: Effect of lithium, samarium and lanthanum dopants. *J. Environ. Chem. Eng.* 10 (2), 107259. doi:10.1016/j.jece.2022.107259

Siakavelas, G. I., Charisiou, N. D., AlKhoori, S., AlKhoori, A. A., Sebastian, V., and Hinder, S. J. (2021). Highly selective and stable nickel catalysts supported on ceria promoted with Sm_2O_3, Pr_2O_3 and MgO for the CO_2 methanation reaction. *Appl. Catal. B Environ.* 282, 119562. doi:10.1016/j.apcatb.2020.119562

Stoian, M., Rogé, V., Lazar, L., Maurer, T., Védrine, J. C., Marcu, I. C., et al. (2021). Total oxidation of methane on oxide and mixed oxide ceria-containing catalysts. *Catalysts* 11 (4), 427. doi:10.3390/catal11040427

Sun, L. L., Wang, Y., Wang, C. M., Xie, Z. K., Guan, N. J., Li, L. D., et al. (2021). Water-involved methane-selective catalytic oxidation by dioxygen over copper zeolites. *Chem* 7 (6), 1557–1568. doi:10.1016/j.chempr.2021.02.026

Sun, Y. N., Liu, J. W., Song, J. J., Huang, S. S., Yang, N. T., Zhang, J., et al. (2016). Exploring the effect of Co_3O_4 nanocatalysts with different dimensional architectures on methane combustion. *ChemCatChem* 8 (3), 540–545. doi:10.1002/cctc.201501056

Sushkevich, V. L., Palagin, D., Ranocchiari, M., and van Bokhoven, J. A. (2017). Selective anaerobic oxidation of methane enables direct synthesis of methanol. *Science* 356, 523–527. doi:10.1126/science.aam9035

Tang, J. J., and Liu, B. (2016). Reactivity of the Fe_2O_3 (0001) surface for methane oxidation: A GGA+ U study. *J. Phys. Chem. C* 120 (12), 6642–6650. doi:10.1021/acs.jpcc.6b00374

Tang, W., Hu, Z., Wang, M., Stucky, G. D., Metiu, H., McFarland, E. W., et al. (2010). Methane complete and partial oxidation catalyzed by Pt-doped CeO_2. *J. Catal.* 273 (2), 125–137. doi:10.1016/j.jcat.2010.05.005

Tang, X. F., Li, J. H., and Hao, J. M. (2008). Synthesis and characterization of spinel Co_3O_4 octahedra enclosed by the {111} facets. *Mat. Res. Bull.* 43 (11), 2912–2918. doi:10.1016/j.materresbull.2007.12.009

Tao, F. F., Shan, J. J., Nguyen, L., Wang, Z. Y., Zhang, S. R., Zhang, L., et al. (2015). Understanding complete oxidation of methane on spinel oxides at a molecular level. *Nat. Commun.* 6, 7798. doi:10.1038/ncomms8798

Teng, F., Su, X., and Wang, X. (2019). Can China peak its non-CO_2 GHG emissions before 2030 by implementing its nationally determined contribution? *Environ. Sci. Technol.* 53, 12168–12176. doi:10.1021/acs.est.9b04162

Tepamatr, P., Laosiripojana, N., and Charojrochkul, S. (2016). Water gas shift reaction over monometallic and bimetallic catalysts supported by mixed oxide materials. *Appl. Catal. A General* 523, 255–262. doi:10.1016/j.apcata.2016.06.023

Toscani, L. M., Curyk, P. A., Zimicz, M. G., Halac, E. B., Saleta, M. E., Lamas, D. G., et al. (2019). Methane catalytic combustion over CeO_2-ZrO_2-Sc_2O_3 mixed oxides. *Appl. Catal. A General* 587, 117235. doi:10.1016/j.apcata.2019.117235

Trimm, D. L., and Lam, C. W. (1980). The combustion of methane on platinum-alumina fibre catalysts-I: Kinetics and mechanism. *Chem. Eng. Sci.* 35 (6), 1405–1413. doi:10.1016/0009-2509(80)85134-7

Trovarell, A. (2002). *Catalysis by ceria and related materials*. London: Imperial College Press.

Vedrine, J. C., Millet, J. M. M., and Volta, J. C. (1996). Molecular description of active sites in oxidation reactions: Acid-base and redox properties, and role of water. *Catal. Today* 32 (1-4), 115–123. doi:10.1016/S0920-5861(96)00185-X

Veldsink, J. W., Versteeg, G. F., and van Swaaij, W. P. M. (1995). Intrinsic kinetics of the oxidation of methane over an industrial copper(II) oxide catalyst on a γ-alumina support. *Chem. Eng. J. Biochem. Eng. J.* 57, 273–283. doi:10.1016/0923-0467(94)02872-8

Vickers, S. M., Gholami, R., Smith, K. J., and MacLachlan, M. J. (2015). Mesoporous Mn- and La-doped cerium oxide/cobalt oxide mixed metal catalysts for methane oxidation. *ACS Appl. Mat. Interfaces* 7 (21), 11460–11466. doi:10.1021/acsami.5b02367

Wang, C. H., and Lin, S. S. (2004). Study on catalytic incineration of methane using Cr_2O_3/γ-Al_2O_3 as the catalyst. *J. Environ. Sci. Health Part A* 39 (6), 1631–1641. doi:10.1081/ese-120037859

Wang, F. G., Zhang, L. J., Xu, L. L., Deng, Z. Y., and Shi, W. D. (2017). Low temperature CO oxidation and CH_4 combustion over Co_3O_4 nanosheets. *Fuel* 203, 419–429. doi:10.1016/j.fuel.2017.04.140

Wang, H. W., Li, J. L., Liu, W. G., Xu, X., Wei, X. F., Chao, L., et al. (2019). Enhancing catalytic CH_4 oxidation over Co_3O_4/SiO_2 core-shell catalyst by substituting Co^{2+} with Mn^{2+}. *J. Dispers. Sci. Technol.* 42 (1), 82–92. doi:10.1080/01932691.2019.1661257

Wang, Q., Peng, Y., Fu, J., Kyzas, G. Z., Billah, S. M. R., An, S. Q., et al. (2015). Synthesis, characterization, and catalytic evaluation of Co_3O_4/γ-Al_2O_3 as methane combustion catalysts: Significance of Co species and the redox cycle. *Appl. Catal. B Environ.* 168-169, 42–50. doi:10.1016/j.apcatb.2014.12.016

Wang, T., Wang, J. Y., Sun, Y. M., Duan, Y., Sun, S. N., Hu, X., et al. (2019). Origin of electronic structure dependent activity of spinel $ZnNi_xCo_{2-x}O_4$ oxides for complete methane oxidation. *Appl. Catal. B Environ.* 256, 117844. doi:10.1016/j.apcatb.2019.117844

Wang, X. Y., Liu, Y., Zhang, Y. Y., Zhang, T. H., Chang, H. Z., Zhang, Y. F., et al. (2018). Structural requirements of manganese oxides for methane oxidation: XAS spectroscopy and transition-state studies. *Appl. Catal. B Environ.* 229, 52–62. doi:10.1016/j.apcatb.2018.02.007

Wang, Y. N., Zhang, R. J., and Yan, B. H. (2022). Ni/$Ce_{0.9}Eu_{0.1}O_{1.95}$ with enhanced coke resistance for dry reforming of methane. *J. Catal.* 407, 77–89. doi:10.1016/j.jcat.2022.01.020

Wang, Y. Q., Rosowski, F., Schlögl, R., and Trunschke, A. (2022). Oxygen exchange on vanadium pentoxide. *J. Phys. Chem. C* 126, 3443–3456. doi:10.1021/acs.jpcc.2c00174

Wang, Z. X., Lin, J., Xu, H., Zheng, Y., Xiao, Y. H., Zheng, Y., et al. (2021). Zr-doped NiO nanoparticles for low-temperature methane combustion. *ACS Appl. Nano Mat.* 4, 11920–11930. doi:10.1021/acsanm.1c02487

Wasalathanthri, N. D., Poyraz, A. S., Biswas, S., Meng, Y., Kuo, C.-H., Kriz, D. A., et al. (2015). High-performance catalytic CH_4 oxidation at low temperatures: Inverse micelle synthesis of amorphous mesoporous manganese oxides and mild transformation to K_2-xMn_8O_{16} and ϵ-MnO_2. *J. Phys. Chem. C* 119 (3), 1473–1482. doi:10.1021/jp5108558

Wu, H. C., and Ku, Y. (2018). Enhanced performance of chemical looping combustion of methane with Fe_2O_3/Al_2O_3/TiO_2 oxygen carrier. *RSC Adv.* 8, 39902–39912. doi:10.1039/c8ra07863g

Wu, H., Pantaleo, G., Di Carlo, G., Guo, S., Marcì, G., Concepción, P., et al. (2015). Co_3O_4 particles grown over nanocrystalline CeO_2: Influence of precipitation agents and calcination temperature on the catalytic activity for methane oxidation. *Catal. Sci. Technol.* 5 (3), 1888–1901. doi:10.1039/c4cy01158a

Xu, J., Zhang, Y., Liu, Y., Fang, X., Xu, X., and Liu, W. (2019). Optimizing the reaction performance of $La_2Ce_2O_7$-based catalysts for oxidative coupling of methane (OCM) at lower temperature by lattice doping with Ca cations. *Eur. J. Inorg. Chem.* 2, 183–194. doi:10.1002/ejic.201801250

Xu, X. L., Li, L., Yu, F., Peng, H. G., Fang, X. Z., Wang, X., et al. (2017). Mesoporous high surface area NiO synthesized with soft templates: Remarkable for catalytic CH_4 deep oxidation. *Mol. Catal.* 441, 81–91. doi:10.1016/j.mcat.2017.08.005

Yang, L., Huang, J. X., Ma, R., You, R., Zeng, H., Rui, Z. B., et al. (2019). Metal-organic framework-derived IrO_2/CuO catalyst for selective oxidation of methane to methanol. *ACS Energy Lett.* 4 (12), 2945–2951. doi:10.1021/acsenergylett.9b01992

Yang, L. Q. Q., Heinlein, J., Hua, C., Gao, R. X., Hu, S., Pfefferle, L. D., et al. (2022). Emerging dual-functional 2D transition metal oxides for carbon capture and utilization: A review. *Fuel* 324, 124706. doi:10.1016/j.fuel.2022.124706

Yang, R. J., Guo, Z. J., Cai, L. X., Zhu, R. S., Fan, Y. Y., Zhang, Y. F., et al. (2021). Investigation into the phase-activity relationship of MnO_2 nanomaterials toward ozone-assisted catalytic oxidation of toluene. *Small* 17 (50), 2103052. doi:10.1002/smll.202103052

Ye, Y. C., Zhao, Y. T., Ni, L. L., Jiang, K. D., Tong, G. X., Zhao, Y. L., et al. (2016). Facile synthesis of unique NiO nanostructures for efficiently catalytic conversion of CH_4 at low temperature. *Appl. Surf. Sci.* 362, 20–27. doi:10.1016/j.apsusc.2015.11.213

Yu, Q., Liu, C. X., Li, X. Y., Wang, C., Wang, X. X., Cao, H. J., et al. (2020). N-doping activated defective Co_3O_4 as an efficient catalyst for low-temperature methane oxidation. *Appl. Catal. B Environ.* 269, 118757. doi:10.1016/j.apcatb.2020.118757

Yu, Q., Wang, C., Li, X. Y., Li, Z., Wang, L., Zhang, Q., et al. (2019). Engineering an effective MnO_2 catalyst from $LaMnO_3$ for catalytic methane combustion. *Fuel* 239, 1240–1245. doi:10.1016/j.fuel.2018.11.094

Yuan, X. Z., Chen, S. Y., Chen, H., and Zhang, Y. C. (2013). Effect of Ce addition on Cr/γ-Al_2O_3 catalysts for methane catalytic combustion. *Catal. Commun.* 35, 36–39. doi:10.1016/j.catcom.2013.02.005

Zasada, F., Janas, J., Piskorz, W., Gorczyńska, M., and Sojka, Z. (2017). Total oxidation of lean methane over cobalt spinel nanocubes controlled by the self-adjusted redox state of the catalyst: Experimental and theoretical account for

interplay between the Langmuir-hinshelwood and mars-van krevelen mechanisms. *ACS Catal.* 7 (4), 2853–2867. doi:10.1021/acscatal.6b03139

Zedan, A. F., and AlJaber, A. S. (2019). Combustion synthesis of non-precious CuO-CeO_2 nanocrystalline catalysts with enhanced catalytic activity for methane oxidation. *Materials* 12 (6), 878. doi:10.3390/ma12060878

Zhang, K., Peng, X. B., Cao, Y. N., Yang, H. G., Wang, X. Y., Zhang, Y. Y., et al. (2019). Effect of MnO_2 morphology on its catalytic performance in lean methane combustion. *Mat. Res. Bull.* 111, 338–341. doi:10.1016/j.materresbull.2018.11.023

Zhang, X., Jin, X., Bao, L. R., Zhang, M. C., Song, R. M., Yu, W., et al. (2021). Construction of defective cobalt oxide for methane combustion by oxygen vacancy engineering. *New J. Chem.* 45 (28), 12655–12660. doi:10.1039/d1nj01296g

Zhang, X. Y., House, S. D., Tang, Y., Nguyen, L., Li, Y. T., Opalade, A. A., et al. (2018). Complete oxidation of methane on NiO nanoclusters supported on CeO_2 nanorods through synergistic effect. *ACS Sustain. Chem. Eng.* 6, 6467–6477. doi:10.1021/acssuschemeng.8b00234

Zhang, Y. G., Qin, Z. F., Wang, G. F., Zhu, H. Q., Dong, M., Li, S. N., et al. (2013). Catalytic performance of MnO_x-NiO composite oxide in lean methane combustion at low temperature. *Appl. Catal. B Environ.* 129, 172–181. doi:10.1016/j.apcatb.2012.09.021

Zhang, Y., Xu, J., Xu, X., Xi, R., Liu, Y., and Fang, X. (2020). Tailoring $La_2Ce_2O_7$ catalysts for low temperature oxidative coupling of methane by optimizing the preparation methods. *Catal. Today* 355, 518–528. doi:10.1016/j.cattod.2019.06.060

Zheng, Y. F., Yu, Y. Q., Zhou, H., Huang, W. Z., and Pu, Z. Y. (2020). Combustion of lean methane over Co_3O_4 catalysts prepared with different cobalt precursors. *RSC Adv.* 10 (8), 4490–4498. doi:10.1039/c9ra09544f

Zheng, Y., Wang, C., Li, J. J., Zhong, F. L., Xiao, Y. H., Jiang, L. L., et al. (2020). Enhanced methane oxidation over Co_3O_4-In_2O_3-x composite oxide nanoparticles via controllable substitution of Co^{3+}/Co^{2+} by In^{3+} Ions. *ACS Appl. Nano Mat.* 3, 9470–9479. doi:10.1021/acsanm.0c02075

Zhong, L., Fang, Q. Y., Li, X., Li, Q., Zhang, C., Chen, G., et al. (2019). SO_2 resistance of Mn-Ce catalysts for lean methane combustion: Effect of the preparation method. *Catal. Lett.* 149 (12), 3268–3278. doi:10.1007/s10562-019-02896-3

Zhu, Y. X., Murwani, I. K., Zhou, C. J., Kemnitz, E., and Xie, Y. C. (2003). Isotopic studies of Sn-Cr binary oxide catalysts for methane total oxidation. *Catal. Lett.* 85 (3-4), 205–211. doi:10.1023/A:1022197830984

Zuo, Z., Ramírez, P. J., Senanayake, S. D., Liu, P., and Rodriguez, J. A. (2016). Low-temperature conversion of methane to methanol on CeO_x/Cu_2O catalysts: Water controlled activation of the C-H bond. *J. Am. Chem. Soc.* 138 (42), 13810–13813. doi:10.1021/jacs.6b08668